Constraining a land surface model with multiple observations by application of the MPI-Carbon Cycle Data Assimilation System

G. J. Schürmann[a], T. Kaminski[b,d], C. Köstler[a], N. Carvalhais[a], M. Voßbeck[b,d], J. Kattge[a], R. Giering[c], C. Rödenbeck[a], M. Heimann[a], and S. Zaehle[a]

[a]Max Planck Institute for Biogeochemistry, Hans-Knöll-Str. 10, 07745, Jena, Germany
[b]The Inversion Lab, Hamburg
[c]FastOpt, Hamburg
[d]previously at FastOpt, Hamburg

Correspondence to: G. Schürmann(gschuer@bgc-jena.mpg.de) and S. Zaehle (soenke.zaehle@bgc-jena.mpg.de)

Abstract. We describe the Max Planck Institute Carbon Cycle Data Assimilation System (MPI-CCDAS) built around the tangent-linear version of the land surface scheme of the MPI-Earth System Model v1 (JSBACH). The simulated terrestrial biosphere processes (phenology and carbon balance) were constrained by observations of the fraction of absorbed photosynthetically active radiation (TIP-FAPAR product) and by observations of atmospheric CO_2 at a global set of monitoring stations for the years 2005 - 2009. When constrained by TIP-FAPAR alone, the system successfully, and computationally efficiently, improved simulated growing season average FAPAR, as well as its seasonality in the Northern extra-tropics. When constrained by atmospheric CO_2 observations, global net and gross carbon fluxes were improved, although the system tended to underestimate tropical productivity. Assimilating both data streams jointly allowed the MPI-CCDAS to match both observations (TIP-FAPAR and atmospheric CO_2) equally well as the single data stream assimilation cases, therefore overall increasing the appropriateness of the resultant biosphere dynamics and underlying parameter values. Our study thus demonstrates the value of multiple-data stream assimilation for the simulation of terrestrial biosphere dynamics and highlights the potential role of remote sensing data, here the TIP-FAPAR product in stabilising the strongly underdetermined atmospheric inversion problem posed by atmospheric transport and CO_2 observations alone. The constraint on regional gross and net CO_2 flux patterns is limited through the parametrisation of the biosphere model. We expect improvement on that aspect through a refined initialisation strategy and inclusion of further biosphere observations as constraints.

1 Introduction

Estimates of the net carbon balance of the terrestrial biosphere are highly uncertain, because the net balance cannot be directly observed at large spatial scales (Le Quéré et al., 2015). Studies aiming to quantify the contemporary global carbon cycle therefore either infer the terrestrial carbon budget as a residual of the arguably better constrained other components of the global carbon budget (Le Quéré et al., 2015), or rely on measurements of atmospheric CO_2 and the inversion of its atmospheric transport (Gurney et al., 2002). Both approaches have the caveat that they are not able to provide accurate estimates at high spatial resolution, and cannot utilise the broader set of Earth system observations that provide information on terrestrial carbon cycle dynamics (Luo et al., 2012). Further, they are diagnostic by nature, and therefore lack any prognostic capacity.

Ecosystem models integrate existing knowledge of the underlying processes governing the net terrestrial carbon balance and have such a prognostic capacity. Since they simulate all major aspects of the terrestrial carbon cycle, they can - in principle - benefit from the broader set of Earth system observations. However, studies comparing different land surface models show a large spread of estimates of the seasonal and annual net land-atmosphere carbon exchange and their trends (Piao et al., 2013; Sitch et al., 2015). This uncertainty is one of the primary causes for discrepancies in future projections of stand-alone terrestrial biosphere models (Sitch et al., 2008), and coupled carbon cycle climate model projec-

tions (Anav et al., 2013; Friedlingstein et al., 2014) for the 21st century. Next to the uncertainty due to different climate forcing (Jung et al., 2007; Dalmonech et al., 2015) and alternative model formulations (Sitch et al., 2015), the uncertainty about the parameter values of the mathematical representation of key carbon cycle processes in these models are an important source of the model spread (Knorr and Heimann, 2001; Zaehle et al., 2005; Booth et al., 2012). This parametric uncertainty can be as large as the differences between models. The spread among models limits our ability to provide further constraints of the net terrestrial carbon uptake.

A potential route to reduce parameter and process-formulation related uncertainties in the estimates of the terrestrial carbon cycle is to systematically integrate the increasing wealth of globally distributed carbon cycle observations into models through data assimilation methods. A broad overview of potential observations and methodological choices is given in Raupach et al. (2005). Knorr and Kattge (2005) investigated the use of a Monte-Carlo approach for data assimilation with global models and suggested that the computational burden (run time) is too large to allow its use with a comprehensive land surface model and a reasonable number of parameters in the optimisation. Notwithstanding this constraint, for a reduced set of parameters Ziehn et al. (2012) managed to successfully apply a Monte Carlo algorithm to the BETHY model in global set-up, albeit with limited process representations. Since computational run time is still a limiting factor in global carbon cycle data assimilation, the development of a relatively "fast" system is advantageous over other assimilation methods. A computationally more efficient method is to to use gradient-based methods. For instance, approximating the gradient with finite differences,Saito et al. (2014) performed assimilation of several data streams with the VISIT model. An alternative to finite difference is to calculate the gradient precisely by a tangent-linear or adjoint version of the biosphere model. A prototype of such a carbon cycle data assimilation system (CCDAS) based on an advanced variational data assimilation scheme and a prognostic terrestrial carbon flux model (BETHY; Knorr 1997, 2000) has demonstrated the potential to effectively constrain the simulated carbon cycle with observations of atmospheric CO_2 (Rayner et al., 2005; Scholze et al., 2007; Kaminski et al., 2013). Conceptually similar systems have been built for other global biosphere models. For example, Luke (2011) constrained the phenology of the JULES model with the MODIS collection 5 leaf area index product and Kuppel et al. (2012, 2013) applied the ORCHIDEE model at a series of FLUXNET-sites to estimate process parameters across these sites and further demonstrated the usefulness of the approach to improve globally modelled CO_2.Bacour et al. (2015) assimilate different FAPAR observations with the ORCHIDEE model (in-situ and satellite) at selected sites and report a large influence on the results depending on the FAPAR-product. Forkel et al. (2014) assimilated FAPAR into the model LPJmL to assess long term control on vegetation greenness. Kaminski et al. (2012) assimilated FAPAR jointly with CO_2 as a constraint and Kato et al. (2013) assimilated the net carbon fluxes and FAPAR jointly at a FLUXNET site.

Here we present the development and first application of the variational data assimilation system built around the JSBACH (Raddatz et al., 2007) model (Max Planck Institute Carbon Cycle Data Assimilation System: MPI-CCDAS), based on the tangent-linear representation of JSBACH. JSBACH is a further development of the BETHY model, providing a more detailed treatment of carbon turnover and storage in the terrestrial biosphere, as well as more detailed treatment of land surface biophysics (Roeckner et al., 2003) and land hydrology (Hagemann and Stacke, 2014), and the land surface scheme of the MPI-Earth System Model (MPI-ESM; Giorgetta et al., 2013).

Our objective with this development is twofold: i) to improve the scope of the original BETHY-CCDAS (see: Kaminski et al., 2013) by including a larger set of terrestrial processes affecting the terrestrial carbon cycle; and ii) to provide a means to constrain the land carbon cycle projections of JSBACH with several data streams, and in hindsight also that of the MPI-ESM. Dalmonech et al. (2015) have shown that the simulated phenolgy, and its seasonal and interannual climate sensitvity, as well as the simulated seasonal net land-atmosphere carbon flux are reasonably robust against climate biases in the MPI-ESM. One can therefore expect that improvements of these aspects made with the MPI-CCDAS driven by observed meteorology will be maintained in the coupled Earth system model. Further, at the example of assimilating atmospheric CO_2 and TIP-FAPAR, we demonstrate the mutual benefit of the two data streams in constraining parameters in JSBACH.

We first provide a technical description of the MPI-CCDAS system. We then demonstrate the capacity of the MPI-CCDAS system to simultaneously integrate atmospheric CO_2 observations and the fraction of absorbed photosynthetically active radiation (FAPAR) recorded from satellites, which constrains the seasonality of the phenology, and assesses the relative effect of the constraint from these two data streams on parameter values and modelled fluxes.

2 Description of MPI-CCDAS

2.1 CCDAS-Method

The MPI-CCDAS relies on a variational data assimilation approach to estimate a set of model parameters. In the following we give a brief overview of this method, and refer for a detailed description to Kaminski et al. (2013). To take account of the uncertainty inherent in the description of observed and simulated variables the method operates on probability density functions (PDFs). It is conveniently formulated in a Gaussian framework and uses the combined infor-

mation provided by the model $M(\boldsymbol{p})$ and the observations $\boldsymbol{d}$ to update a PDF that describes the prior state of information on the parameter vector $\boldsymbol{p}$ (more precisely on the control vector, which is a combination the model's process parameters and of initial state variables). This prior control vector is described by the mean $\boldsymbol{p}_{pr}$ and the covariance of its uncertainty $\mathbf{C}_{pr}$. The CCDAS method seeks to minimize the missfit between observed and modelled quantities by minimizing the cost function J

$$J(\boldsymbol{p}) = \frac{1}{2}\left(M(\boldsymbol{p})-\boldsymbol{d}\right)^T \mathbf{C}_d^{-1}\left(M(\boldsymbol{p})-\boldsymbol{d}\right) + \left(\boldsymbol{p}-\boldsymbol{p}_{pr}\right)^T \mathbf{C}_{pr}^{-1}\left(\boldsymbol{p}-\boldsymbol{p}_{pr}\right) \quad (1)$$

where $\mathbf{C}_d$ is the covariance of combined uncertainty in the observations (with mean $\boldsymbol{d}$) and model simulation. The minimum of J, denoted as $\boldsymbol{p}_{po}$ (the posterior control vector), is the maximum likelihood estimate. $\boldsymbol{p}_{po}$ thus balances the misfit between modelled quantities and their observational counterparts over the entire assimilation window, while taking independent prior information on the control vector into account. This means the vector d contains all observations, which act to simulatenously constrain the control vector. In contrast to sequential assimilation schemes, this approach determines a model trajectory through the state space, which, in particular, ensures convervation of mass and energy (see, e.g., Kaminski and Mathieu, 2016).

Technically, J is minimized by a quasi Newton approach with so-called Broyden-Fletcher-Goldfarb-Shanno (BFGS) updates of the Hessian approximation, in the implementation provided by the Numerical Recipes (Press et al., 1992, dfpmin routine). The iterative procedure requires the gradient $\frac{\partial J}{\partial p}$, which is evaluated by the tangent-linear version of the model that was generated by TAF (Giering and Kaminski, 1998) via automatic differentiation (AD: Griewank 1989) of the model's source code. The fundamental modes of AD, forward and reverse, respectively produce tangent-linear and adjoint codes, by application of the chain rule. Unlike the traditional approximation by finite or divided differences of model runs (numerical differentiation), tangent-linear and adjoint codes provide derivative information that is accurate up to machine precision.

The values and uncertainties for the control and observational vectors as well as the model are detailed in the following sub-sections.

2.2 The forward model

The model that is optimised within the MPI-CCDAS is the land surface model JSBACH (Raddatz et al., 2007; Brovkin et al., 2009; Reick et al., 2013; Schneck et al., 2013; Dalmonech and Zaehle, 2013). The model considers ten plant functional types (PFTs: see Table 1). These PFTs are allowed to co-occur within one grid cell on different tiles, but nonetheless share a common water storage. Compared to the aforementioned JSBACH studies, the MPI-CCDAS does not use land-use change and land-use transition nor dynamic vegetation, but uses a multi-layer soil hydrology scheme (Hagemann and Stacke, 2014). JSBACH is typically used within the MPI-ESM (Giorgetta et al., 2013) and calculates the terrestrial storage of energy, water and carbon and its half-hourly exchanges between the atmosphere and the land surface. JSBACH is applied here uncoupled from the atmosphere and forced with reconstructed meteorology (see Sec. 3).

Table 1. Plant functional types that are optimised and the limitations that control the phenological behaviour of the respective functional type.

Plant functional type	Limitations
Tropical evergreen trees (TrBE) Tropical deciduous (TrBS) Raingreen shrubs (RS)	Water
Coniferous evergreen trees (CE) Extra-tropical deciduous trees (ETD) Coniferous deciduous (CD)	Temperature and Daylight
C3-grasses (TeH) C3-crops (TeCr) C4-grasses (TrH) C4-crops (TrCr)	Temperature and Water

The application of gradient-based minimisation procedures is facilitated by a differentiable calculation of $J(\boldsymbol{p})$. According the the chain rule, this ultimately requires all code parts of the forward model that depend on the control variables and impact the cost-function to be differentiable. To improve differentiability, the original phenology scheme, which describes the timing and amount of foliar area based on logistic growth functions (Lasslop, 2011) was replaced by the alternative scheme developed explicitly for this purpose (Knorr et al., 2010) (see Sec. A1). Some further minor modifications were necessary to make the code differentiable. These changes included replacing look-up tables with their continuous formulations, avoiding division by zero in the derivative code (e.g. through differentiation of $\sqrt{0}$ in the forward mode leading to $\frac{1}{\sqrt{0}}$ in the diffentiated code), and reformulating minimum and maximum calculations to allow a smooth transition at the edge. These modifications alter the calculations, however, they were implemented such that the differences in the modelled results compared to the original code is minimal.

2.2.1 Atmospheric transport

To map the net land-atmosphere CO_2 exchange simulated by JSBACH to observations of the atmospheric CO_2-mole fraction, the computation of atmospheric transport is required,

which is done here by the transport model TM3 (Heimann and Körner, 2003). Specifically, we compute the response of monthly mean CO_2 mole fractions $\boldsymbol{c}$ to monthly mean surface fluxes $\boldsymbol{f}$ (extending 2 years back in time).Since the atmospheric transport is linear (in the fluxes), this can be written as:

$$\Delta \boldsymbol{c} = \mathbf{M} \cdot \boldsymbol{f} \quad (2)$$

where $\mathbf{M}$ represents the TM3 responses as a transport matrix.

In the MPI-CCDAS these transport matrices (or Jacobians)are multiplied with the net CO_2 exchange as in Rödenbeck et al. (2003). The net exchange is the sum of the terrestrial fluxes computed by JSBACH and those not computed by JSBACH, i.e. prescribed ocean and fossil fuel fluxes. Biomass burning fluxes are not explicitly included (see also discussion in Sect. 5.5) and these fluxes are consequently mapped to the respiratory part of JSBACH during the assimilation of atmospheric CO_2 The mole fraction at the beginning of this simulation is specified as a globally constant offset CO_2^{offset}, one of the parameters to be estimated. The resulting CO_2-mole fractions can then be directly compared with observed atmospheric CO_2. Limiting the system to one global modifier was motivated by limitation in the computational run time, while an inclusion of an offset depending on the observation locations could be easily implemented. With a spin-up of 2 years for the atmospheric transport, we allow the system to build up the latitudinal gradient of CO_2. After the second year, there is no visible trend in the difference of observed CO_2 at Mauna Loa and South Pole. Thus 2 years are sufficient to spin-up the atmosphere.

For our analysis, we used the Jacobian representation of the TM3 model, version 3.7.24 (Rödenbeck et al., 2003), with a spatial resolution of about 4°x5° (the "fine" grid of TM3 by Heimann and Körner 2003), driven by interannually varying wind fields of the NCEP reanalysis (Kalnay et al., 1996).

2.3 Model parameters

For this study, JSBACH parameters related to the phenology, photosynthesis and land carbon turnover (including initial carbon stocks) are optimized (see appendix A for a more detailed description on the relevant parts of JSBACH). The default prior value and assumed prior Gaussian uncertainty of each parameter and the posterior values from the assimilation experiments are given in Table 2. The choice of these parameters was based on an extensive parameter sensitivity study on a much larger set of parameters across multiple biomes (Schürmann, unpublished results). We retained those parameters, for which we found a significant effect on modelled FAPAR and net CO_2 exchange. In principle, it is possible to add more parameters, which are decisive for other modelled quantities such as soil moisture and which might feed back to our observables. A brief explanation of the parameters involved in this study is given in the following.

The parameters controlling the phenology (Λ_{max}, τ_l, τ_w, T_ϕ, t_c, and ξ) are allowed to take different values for different plant functional types with the exception of ξ, which is valid globally. While Λ_{max} controls the maximum amount of leaves, ξ controls the rate of leaf growth, and τ_l is the time-scale of leaf senescence. T_ϕ and t_c are temperature and day-length tresholds, respectively, controlling the onset and end of vegetation activity. The parameter τ_w controls the shedding of leaves in response of phenology for drought-deciduous PFTs. Soil moisture in JSBACH follows a 5-layer scheme (Hagemann and Stacke, 2014) and is coupled to the vegetation via the phenology and the photosynthesis by influencing actual stomatal conductance. The phenological parameter prior values and uncertainties are taken from Knorr et al. (2010), with the following three exceptions: the water control parameter τ_w required an adaptation to account for the different soil-water formulations in the MPI-ESM compared to BETHY, τ_l for the coniferous evergreen (CE) PFT also has been adapted after preliminary site-scale studies to allow more flexibility in the seasonality of the evergreen-phenology (Schürmann, unpublished results) and, finally, Λ_{max} is left to its default JSBACH parameter value for all PFT's with the exception of the coniferous evergreen (CE) PFT. For this PFT a value of $\Lambda_{max} = 1.7\,\mathrm{m}^2/\mathrm{m}^2$ has been used, because preliminary model tests revealed a large bias in modelled FAPAR in CE-dominated regions, which adversely affected the model results of the carbon cycle.

Photosynthesis in JSBACH follows Farquhar et al. (1980) for C3-plants and Collatz et al. (1992) for C4- plants, with details as described in Knorr and Heimann (2001) and Knorr (1997). To estimate gross assimilation directly, maximum carboxylation rate Vc_{max} and maximum electron transport J_{max} are allowed to vary per PFT. We assume that the observed tight correlation between Vc_{max} and J_{max} is conserved irrespective of the precise value for each PFT (Kattge and Knorr, 2007). Thus, we introduce a single scaling coefficient f_{photos}:

$$Vc_{max} = Vc_{max}^{prior} \cdot f_{photos} \quad (3)$$

$$J_{max} = J_{max}^{prior} \cdot f_{photos} \quad (4)$$

Prior parameter ranges for each PFT were derived from the TRY data-base (Kattge et al., 2011).

Autotrophic respiration in JSBACH follows Knorr (2000) where growth respiration is a fixed fraction (20 %) of the net assimilation. Maintenance respiration scales with dark respiration (with a parameter f_{aut_leaf}) assuming to be coordinated with foliar photosynthetic activity. Net primary production is allocated to either a green or woody pool which turns to three litter pools (above ground green, below ground green and woody) with distinct PFT-specific turnover times. Heterotrophic respiration of these pools responds to temperature according to a $Q10$ formulation (see appendix A). The prior sensitivity studies revealed that the most influential pa-

Table 2. Parameters that are part of the control vector with their prior and posterior values of the global assimilation experiments. Parameters marked with a * are multiplied with their respective value in the model, given in Table D1. The mapping variants are explained in the appendix C: 1: No lower bound; 2: A lower bound at 0 for those parameters that are not allowed to take negative values.

Representation in Eq. 1:		$\mathbf{C}_{pr}$	$\boldsymbol{p}_{pr}$	$\boldsymbol{p}_{po}$				
Parameter(PFT)	**Description**	**Prior sigma**	**Prior**	**JOINT**	**CO2alone**	**FAPARalone**	**Unit**	**Mapping**
Λ_{max} (TrBE)*	Maximum LAI	0.2	1	0.98	0.82	0.84	.	2
Λ_{max} (TrBD)*	Maximum LAI	0.2	1	0.58	0.55	0.63	.	2
Λ_{max} (ETD)*	Maximum LAI	0.2	1	0.98	1.04	1.44	.	2
Λ_{max} (CE)*	Maximum LAI	0.2	1	1.00	0.84	1.01	.	2
Λ_{max} (CD)*	Maximum LAI	0.2	1	0.64	1.31	0.56	.	2
Λ_{max} (RS)*	Maximum LAI	0.2	1	1.33	0.94	1.24	.	2
Λ_{max} (TeH,TeCr)*	Maximum LAI	0.1	1	0.63	0.53	0.61	.	2
Λ_{max} (TrH,TrCr)*	Maximum LAI	0.1	1	0.53	0.49	0.59	.	2
$1/\tau_l$ (ETD)	Leaf shedding time scale	0.01	0.07	0.057	0.057	0.079	d^{-1}	2
$1/\tau_l$ (CE)	Leaf shedding time scale	1e-04	5e-04	0.00067	0.00045	0.00064	d^{-1}	2
$1/\tau_l$ (CD)	Leaf shedding time scale	0.01	0.07	0.068	0.07	0.068	d^{-1}	2
$1/\tau_l$ (TeH,TeCr)	Leaf shedding time scale	0.01	0.07	0.098	0.076	0.079	d^{-1}	2
$1/\tau_l$ (TrH,TrCr)	Leaf shedding time scale	0.01	0.07	0.077	0.07	0.07	d^{-1}	2
τ_w (TrBE)	Water stress tolerance time	30	300	319.82	378.04	286.77	days	2
τ_w (TrBD)	Water stress tolerance time	10	114	107.78	120.84	106.29	days	2
τ_w (RS)	Water stress tolerance time	5	50	49.51	50.02	47.82	days	2
τ_w (TeH,TeCr)	Water stress tolerance time	25	250	222.32	215.22	230.41	days	2
τ_w (TrH,TrCr)	Water stress tolerance time	25	250	276.06	236.32	286.64	days	2
T_ϕ (ETD)	Temperature at leaf onset	1	9.21	7.19	8.63	2.28	°C	1
T_ϕ (CE)	Temperature at leaf onset	1	9.21	7.53	9.01	7.61	°C	1
T_ϕ (CD)	Temperature at leaf onset	1	9.21	0.10	5.53	0.30	°C	1
T_ϕ (TeH,TeCr)	Temperature at leaf onset	0.5	1.92	3.82	2.67	2.78	°C	1
T_ϕ (TrH,TrCr)	Temperature at leaf onset	0.5	1.92	2.50	1.57	1.88	°C	1
t_c (ETD)	Day length at leaf shedding	1	13.37	13.57	13.84	13.60	hours	2
t_c (CE)	Day length at leaf shedding	1	13.37	14.22	13.69	14.12	hours	2
t_c (CD)	Day length at leaf shedding	1	13.37	14.94	13.66	14.73	hours	2
ξ	Initial leaf growth rate	0.03	0.37	0.41	0.38	0.43	d^{-1}	2
f_{photos} (TrBE)*	Photosynthesis rate modifier	0.1	1	0.75	1.02	0.91	.	2
f_{photos} (TrBD)*	Photosynthesis rate modifier	0.1	1	1.07	1.08	0.97	.	2
f_{photos} (ETD)*	Photosynthesis rate modifier	0.02	1	0.99	1.00	1.00	.	2
f_{photos} (CE)*	Photosynthesis rate modifier	0.03	1	0.95	1.00	1.00	.	2
f_{photos} (CD)*	Photosynthesis rate modifier	0.06	1	1.04	1.05	1.00	.	2
f_{photos} (RS)*	Photosynthesis rate modifier	0.1	1	1.01	1.05	1.00	.	2
f_{photos} (TeH)*	Photosynthesis rate modifier	0.1	1	0.96	1.01	0.99	.	2
f_{photos} (TeCr)*	Photosynthesis rate modifier	0.1	1	0.67	0.86	1.00	.	2
f_{photos} (TrH)*	Photosynthesis rate modifier	0.1	1	1.04	1.02	1.06	.	2
f_{photos} (TrCr)*	Photosynthesis rate modifier	0.1	1	0.87	0.94	1.00	.	2
Q_{10}	Temperature sensitivity of resp.	0.15	1.8	1.90	1.81	1.80	.	2
f_{slow}	Multiplier for initial slow pool	0.1	1	0.50	0.51	1.00	.	2
f_{aut_leaf}	Leaf fract. of maintenance resp.	0.1	0.4	0.30	0.35	0.40	.	2
CO_2^{offset}	Initial atmospheric carbon	3	0	0.90	0.85	0.00	ppm	1

rameters controlling Carbon storage on land and partitioning between autotrophic and heterotrophic respiration were the leaf fraction of maintenance respiration (f_{aut_leaf}) and temperature response (Q_{10}) of the carbon pools, which were both included as parameters into the optimisation. The uncertainty of these parameters was based on expert knowledge, and inspired by the works of Mahecha et al. (2010) for $Q10$ and Knorr (2000) for f_{aut_leaf}.

To account for non steady-state conditions of the net carbon flux, we followed the approach of Carvalhais et al. (2008) by estimating a global scaling factor for the size of the initial slow pool f_{slow}. The inclusion of f_{slow} to the optimized parameters allows for the modification of global heterotrophic respiration and hence also an adjustment of the $\mathrm{CO_2}$ growth rate via altering the net carbon flux from or to the atmosphere. However, the limitation is that this does not change the spatial distribution of carbon pools, which remains controlled by the prior parameter values. For this first application of the MPI-CCDAS, the most slowly varying pool has been selected (i.e. the soil carbon pool with a turnover time of 100 years). The initial conditions of other carbon pools were not included in the control vector to avoid the associated increase in the computational burden (e.g. run time). This consequently includes the risk of assigning any misrepresentation of modelled pools sizes to the soil carbon pool and the changes in the carbon pool sizes after the assimilation should be interpreted with care. The uncertainty of f_{slow} has been set to 10 %, reflecting a moderate deviation from equilibrium (but see also discussion in Sect. 5.4). The turnover-time parameters (see Eq. A18) were not included in the assimilation experiment, because their impact on land carbon fluxes was small compared to other parameters (Schürmann, unpublished results) at the time-scale of the MPI-CCDAS (a couple of years).

To account for minor offsets of the MPI-CCDAS with respect to the initial carbon content of the atmosphere, one single offset value CO_2^{offset} is included in the set of estimated parameters. CO_2^{offset} was assumed to not deviate more than a few ppm, and its uncertainty set accordingly.

Uncertainties on all parameters were assumed to be Gaussian and exposed to the assimilation procedure in a form normalized by their prior uncertainty. In order to prevent parameters from attaining physically impossible, negative values, some parameters were constrained at the lower end of the distribution to zero (see Table 2 and appendix C).

2.4 Observational constraints and observation operators

2.4.1 Atmospheric $\mathrm{CO_2}$

Observed atmospheric $\mathrm{CO_2}$ mole fractions were obtained from the flask data/continuous measurements provided by different institutions (e.g. flask data of NOAA/CMDL's sampling network, update of Conway et al. 1994, Japan Meteorological Agency - JMA, Meteorological Service of Canada - MSC, and many others; see Rödenbeck et al. 2003). Stations were selected in order to cover the global latitudinal gradient (Table B1), focussing on remote locations with little imprint of local fluxes. For cross-evaluation, a disjunct set of available station data were used (Table B2). The temporal resolution of the $\mathrm{CO_2}$ original data at the monitoring stations (hourly to daily/weekly) depends on the specific station and were averaged into monthly means.

The MPI-CCDAS compares atmospheric $\mathrm{CO_2}$ at a monthly temporal resolution, considering the sampling of simulated $\mathrm{CO_2}$ abundance at the same time in which measurements were available in order to reduce the representation error. The treatment of the observations of $\mathrm{CO_2}$ and their uncertainties are done as in Rödenbeck et al. (2003). A floor value of 1 ppm is added to this uncertainty, similarly as in Rayner et al. (2005). Ancillary flux fields at monthly resolution were prescribed to represent the ocean (Jena CarboScope pCO2-based mixed layer scheme oc_v1.0 Rödenbeck et al., 2013) and fossil fuel (Emissions Database for Global Atmospheric Research EDGAR, European Commission, Joint Research Centre (JRC)/Netherlands Environmental Assessment Agency (PBL) 2009) net $\mathrm{CO_2}$ fluxes.

2.4.2 TIP-FAPAR

The observations of FAPAR that have been assimilated were specifically derived for this study by the Joint Research Centre Two-stream Inversion Package (JRC-TIP, Pinty et al. 2007). The product was derived by running JRC-TIP on MODIS broadband visible and near-infrared white sky surface albedo input aggregated to the model grid separately for snow-free and snow-like background conditions in a similar way as described for the native 0.01 degree product (Pinty et al., 2011a, b; Clerici et al., 2010; Voßbeck et al., 2010). JRC-TIP has been explicitly designed to deliver products suitable for assimilation into climate and numerical weather prediction models. It is based on an advanced one dimensional two-stream scheme Pinty et al. (2006) that assures a physically consistent solution of the radiative transfer problem in the coupled canopy-soil system. Similar schemes are implemented in most state-of-the-art terrestrial biosphere models (see, e.g. Loew et al., 2014). Uncertainties in the FAPAR data are based on rigorous uncertainty propagation from the MODIS input albedos using first and second derivative information (Voßbeck et al., 2010). A space and time invariant prior (except for the occurrence of snow) is used, i.e. all spatio-temporal variability in the products is derived from the input products (including the MODIS snow flag). In contrast to alternative algorithms there is no variability imposed through (possibly implicit) assumptions, e.g. on land cover (as in Knyazikhin et al., 1999), which avoids inconsistencies, e.g. with the model's own land cover (for more details see Disney et al. (2016)). To reduce biases in the retrieved products through the prior information, the prior is given a

deliberately low weight, e.g. a sigma of 5 for the effective LAI (Pinty et al., 2011a).

We applied two filters on the global FAPAR product to assure that potential model structural errors did not lead to compensating effects in the parameter estimation procedure and thus impede fitting the FAPAR data in other regions. First, owing to the fact that no specific crop-phenology is implemented in JSBACH, grid cells with fractional crop coverage of more than 20 % have been filtered out, as we cannot expect the model to fit cropland phenology. A consequence of this filter is to mask the deciduous broadleaf PFT in the US and Europe, because in these areas, this PFT is collocated in crop-dominated pixels. Hence, the phenological parameters of the deciduous broadleaf PFT are only constrained by observations from other locations - a fact that should be kept in mind when interpreting the deciduous broadleaf parameters. Second, grid-points with correlations between the prior model and the observed FAPAR below 0.2 (i.e. prior phenology exhibits out-of-phase seasonal cycles) have also been filtered out. Together, these filters reduce the overall global coverage of the FAPAR-constraint and thus the number of observations to be fitted (Fig. 1) by 57 %.

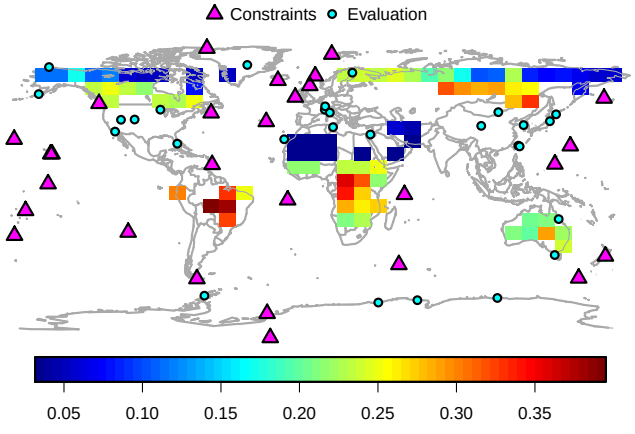

Figure 1. Location of the CO_2 observations (for constraining the model and for evaluation) and the median over the time series of the TIP-FAPAR uncertainties (given with the color-scale) in each pixel acting as constraint.

3 Experimental set-up

The MPI-CCDAS is driven by daily meteorological forcing (air temperature, specific humidity, precipitation, downward short- and longwave radiation, wind speed) obtained from the WATCH forcing data set (Weedon et al., 2014). Annual CO_2 mole fractions of the atmosphere as a forcing for the photosynthesis calculations of JSBACH were prescribed according to Sitch et al. (2015). Vegetation distribution (Fig. E1) and other surface characteristics are derived from Pongratz et al. (2008). Although the MPI-CCDAS is flexible to be run at any spatial resolution, for computational efficiency, we have set-up the MPI-CCDAS at a coarse spatial resolution of about 8°x10°, even though the atmospheric transport itself was simulated at 4°x5°, because the precomputed Jacobians have been calculated at that resolution.

For the water and carbon cycle state-variables of JSBACH, the following spin up procedure was applied: First, an equilibrium was achieved through an integration over the period 1979-1989 with corresponding meteorological forcing and atmospheric CO_2 mole fractions of 1979. Starting from this equilibrium state, a transient integration from 1979 to 2003 followed. The final state of 2003 was then taken as the initial condition for all MPI-CCDAS experiments. This spin-up procedure used the prior parameter values, i.e. it was not part of the assimilation loop for the parameter estimation. To allow a direct control of the non-equilibrium states of the carbon pools, the initial soil carbon pool (at the end of the spin-up procedure) was multiplied by a global scaling factor that is part of the parameter estimation procedure (see Sect. 2.3).

The MPI-CCDAS itself was run for the years 2003 - 2011, i.e. parameters were left free to adapt to the observational constraints. The first two years (2003 to 2004) allowed the system to build a spatial gradient in the simulated atmospheric CO_2 mole fractions. In the following years (2005 to 2009) the observational constraints were active. For the consecutive two years (2010 to 2011), the constraints were inactive and the observations were used to evaluate the MPI-CCDAS with posterior parameters in hindcast-model.

As evaluation statistics, we used the correlation, bias, root mean squared error and the Nash-Sutcliffe model efficiency (NSE). The latter is defined as:

$$NSE = 1 - \frac{\sum_i (d_i - m_i)^2}{\sum_i \left(d_i - \overline{d_i}\right)^2} \quad (5)$$

where the index i denotes individual pairs of observation (d) and model output (m) and an overbar the arithmetic mean. $NSE = 1$ indicates a perfect model and for all $NSE < 0$ the mean of the observations is a better predictor than the model itself.

Our study follows a factorial design to assess the benefit of each data stream, but also to evaluate the potential of assimilating more than one data stream and its effect on the carbon cycle. Therefore, we conducted three experiments: two experiment assimilating each one data stream alone (CO2alone using only CO_2 and FAPARalone using only TIP-FAPAR) and one experiment assimilating both data streams simultaneously (JOINT), with each data stream equally weighted in the cost function (Eq. 1).

Table 3. Characteristics of the assimilation experiments. The prior and posterior cost-function values and the contribution of FAPAR, CO_2 and the prior (second term in Eq. 1) to the posterior cost-function value are given as well as the norm of the gradient and the number of observations acting as a constraint and the number of iterations of the assimilation

Experiment name	Prior cost	Posterior cost	FAPAR cost	CO_2 cost	Parameter cost	Prior norm of the gradient	Posterior norm of the gradient	Number of observations	Number of iterations
CO2alone	1922	344	0	287	57	12196	14.8	1524	69
FAPARalone	1431	723	626	0	97	208	0.7	3189	29
JOINT	3352	1102	682	309	112	12162	6.1	4713	69

4 Results

4.1 Performance of the assimilation

The application of the MPI-CCDAS to the given problem (FAPARalone, CO2alone, or JOINT) was successful within an appropriate number (tens to hundreds) of iterations (with run-times of 1 - 2 months), increasing from FAPARalone (using only TIP-FAPAR), to CO2alone (using only CO_2), and JOINT (using both observations simultaneously as a constraint; Table 3): For all three assimilation experiments, the value of the cost-function was considerably reduced, while the posterior parameter values remained in physically plausible ranges, even though a few (e.g.: T_ϕ of the coniferous deciduous phenotype) deviate strongly from the prior values (Table 2). For FAPARalone, the value of the cost function was almost halved between prior and posterior run. Even stronger reductions of the cost function were obtained in the other two experiments using also CO_2 (Table 3). Several statistics comparing the posterior model with observations for FAPAR and CO_2 (Tables 4 and 5) show that the model performance of the JOINT experiment was comparable to the performance of the two single data-stream experiments relative to the assimilated quantity. While the JOINT assimilation captured the main features of both data sources, the single data-stream assimilation experiments either showed no improvement with respect to the other data stream (such as the CO2alone case for FAPAR), or even a degradation (such as the FAPARalone case for CO_2). Overall, these results suggest that both data streams can be successfully assimilated jointly with the MPI-CCDAS.

During the assimilation procedure, the norm of the gradient[1] $\frac{\partial J}{\partial p}$ (see Eq. 1) was considerably reduced by 3 - 4 orders of magnitude (Table 3). The behaviour was such that during the first tens of iterations of the assimilation procedure, the cost as well as the norm of the gradient were considerably reduced. Also the parameter values changed the most in this initial phase of the assimilation. However, they also changed in later iterations without substantial reductions in the cost function or the norm of the gradient. The assimilation then finally stopped, because the changes to the parameters became too small. In the following we discuss the performance of the assimilation with respect to FAPAR and CO_2 in detail.

[1]The norm of a vector $\boldsymbol{v}$ is: $\|\boldsymbol{v}\| = \sqrt{\boldsymbol{v} \cdot \boldsymbol{v}}$

4.2 Phenology

The statistics of the comparison with the TIP-FAPAR data sets shows an improvement of the model-data fit for all experiments relative to the prior model (Table 4), which as expected is strongest when using FAPAR (FAPARalone and JOINT) as a constraint.

One important reason for the improvement was a general reduction in modelled growing-season average FAPAR simulated by the MPI-CCDAS compared to the prior run. This decrease in FAPAR was mostly driven by a reduction of globally averaged foliar area of 0.41 $\mathrm{m^2 m^{-2}}$ for the JOINT experiment (0.34 $\mathrm{m^2 m^{-2}}$ for FAPARalone and 0.59 $\mathrm{m^2 m^{-2}}$ for CO2alone). Almost all PFTs contributed to the decrease in FAPAR following a reduction in the maximum leaf area index parameter (Λ_{max}) for tropical deciduous forests, needleleaf deciduous forests, as well as herbaceous PFTs (crops and grasses). The water-stress parameter τ_w played a secondary role in the leaf area reduction by affecting the maximum leaf-area for drought responsive PFTs (see Table 1). The concurrent increase of foliar area for extra-tropical deciduous and rain green shrubs only plays a minor role in the model-data agreement, since these PFTs only cover a small fraction of the global land area.

In regions with a strong temperature control of phenology, the assimilation did not only change the average LAI during the growing season. As demonstrated by the enhanced correlation and model efficiency of the MPI-CCDAS with respect to the TIP-FAPAR data (Table 4), also the timing of onset and end of the growing season was improved. This improvement was mostly the result of adjusting the parameters T_ϕ and t_c, which are temperature and day-length criteria that determine when the vegetation switches from the dormant to the active phase. In particular, the assimilation reduced the temperature control parameter T_ϕ, which led to an earlier onset of the growing season in the extra-tropical deciduous broadleaf and deciduous needleleaf PFTs. For the deciduous needleleaf forests the assimilation procedure also resulted in an earlier end of the growing season, in accordance with the observations (see Fig. 2 for an example). The parameters controlling the phenological timing of other PFTs were not strongly al-

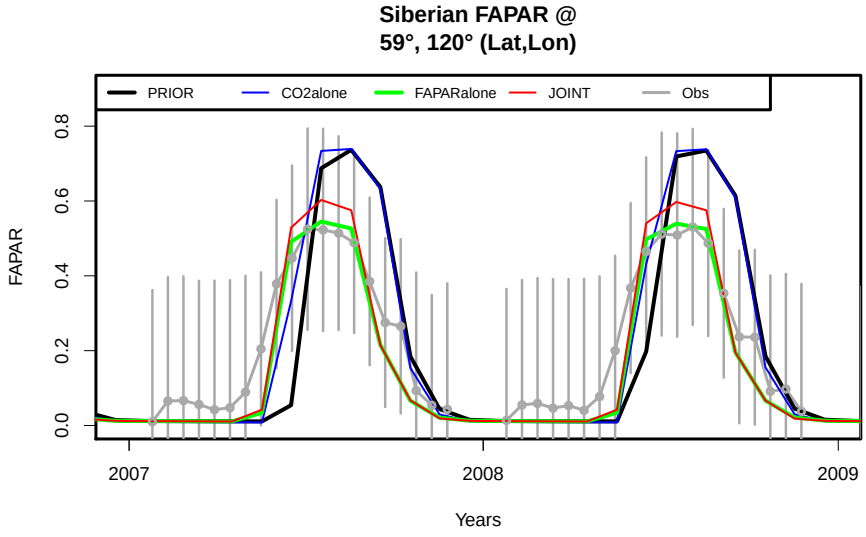

Figure 2. Example time-series of FAPAR for an East Siberian pixel dominated by the CD-PFT to demonstrate the improvement in the timing of the phenology after the assimilation. TIP-FAPAR observations are given with their mean (dots) and $1 \cdot \sigma$ uncertainties (vertical lines).

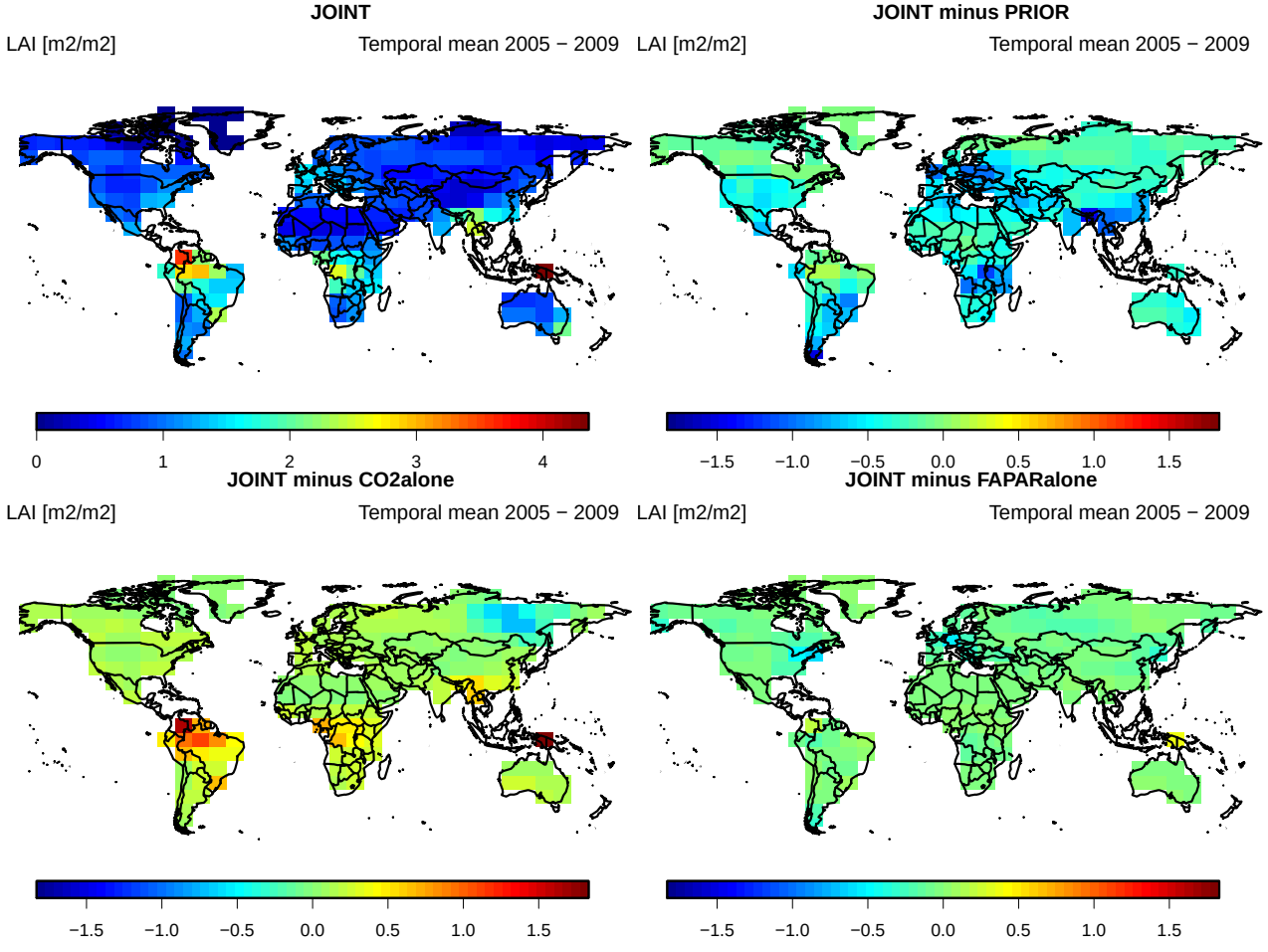

Figure 3. Temporally averaged global LAI of the JOINT experiment and differences of the other experiments to the JOINT case.

Table 4. Performance of the prior and posterior models compared with TIP-FAPAR observations (applying the same data quality screening as for the assimilation). The assimilation period (2005 - 2009) as well as a subsequent evaluation period (2010/2011) is shown. Abbreviations are: Bias: Model - Observations, Corr: Correlation, RMSE: Root mean squared error, NSE: Nash Sutcliffe model efficiency.

	2005 - 2009				2010/2011			
	Corr	Bias	RMSE	NSE	Corr	Bias	RMSE	NSE
PRIOR	0.60	0.069	0.19	0.10	0.61	0.075	0.19	0.12
CO2alone	0.66	-0.072	0.17	0.31	0.67	-0.074	0.17	0.31
FAPARalone	0.72	-0.014	0.14	0.51	0.73	-0.013	0.14	0.52
JOINT	0.71	-0.022	0.14	0.49	0.72	-0.022	0.14	0.50

tered by the assimilation, which - at the monthly temporal resolution of the satellite data analysed here - led to no observable modification of the temporal behaviour of FAPAR. Notably, also the CO2alone experiment showed some improvement in the correlation and model efficiency compared to TIP-FAPAR, although this experiment did not use the TIP-FAPAR data as a constraint. This suggests that the seasonal cycle of CO_2 bears some constraint on the timing of northern extra-tropical phenology.

While the FAPARalone assimilation run performs best compared with TIP-FAPAR (Table 4), the FAPARalone and JOINT assimilation runs are fairly similar (though not identical) with respect to the simulated FAPAR. The temporally averaged LAI (Fig. 3) demonstrates the overall similarity between the FAPARalone and JOINT experiments. This similarity is also reflected in the parameter values of the phenology: the parameters of FAPARalone and JOINT often were closer to each other than to CO2alone (Table 2). An example for this are the tropical evergreen tree PFTs, for which parameters of the JOINT and FAPARalone experiment are different while the modelled foliar area is very similar. A further explanation for this feature highlighting the importance of multi-data stream assimilation is given in Sec. 4.4.1. The most pronounced differences between the JOINT and FAPARalone experiment, leading also to the differences in the globally averaged foliar area, arose at locations where TIP-FAPAR data were not used as constraints in e.g. crop dominated pixels (where also the extra-tropical deciduous tree (ETD) PFT covered a substantial part of the grid-cell).

Larger differences in FAPAR were obtained with the CO2alone and JOINT experiments (Table 4 and Fig. 3). The CO2alone experiment showed the smallest LAI, and thus the smallest FAPAR. This feature is especially pronounced in tropical regions, where the decrease is driven by the water-control parameter τ_w and the maximum foliar area Λ_{max}. This pattern is countered by larger foliar area than the JOINT experiment for coniferous deciduous trees, driven by the parameter Λ_{max} which is increased for CO2alone, but decreased for the other two experiments. A likely explanation of this behaviour is given in Sect. 4.4.2.

4.3 Atmospheric CO_2

The assimilation procedure strongly reduced the misfit between observed and modelled atmospheric mole fraction of CO_2 when using CO_2 as a constraint (Table 5). This was true for the seasonal cycle, the seasonal cycle's amplitude and the 5-years trend (Fig. 4 and 5). Conversely, the FAPARalone experiment showed a strong deterioration of the simulated atmospheric CO_2 metrics compared to the prior model. Notwithstanding an improvement of the seasonal cycle amplitude of atmospheric CO_2 (Fig. 5), the 5-years trend of atmospheric CO_2 was much less conforming to the observations, leading to a much faster increase in CO_2 than observed (Table 5 and Fig. 4). Notably, introducing TIP-FAPAR as an additional constraint in the JOINT experiment did allow the MPI-CCDAS to match both the atmospheric CO_2 data and the TIP-FAPAR product: the simulated monthly CO_2 mole fractions of the JOINT and CO2alone experiment are almost identical for most sites (Table 5 and Fig. 4 and 5).

The improvement of the simulated atmospheric CO_2 for the CO2alone and JOINT assimilation run persisted for the two years following the assimilation period, in which the model was run in a hindcast mode (driven by reconstructed meteorology), with only minor degradation in model performance (Table 5). Both experiments clearly outperform the prior model, which is most obvious in the improvement of the Nash-Sutcliffe model efficiency for the hindcast period.

The comparison of the simulated posterior atmospheric CO_2 mole fractions at the evaluation stations showed a general improvement in the performance measures, with substantial improvements in the simulated bias, RMSE and Nash-Sutcliffe model efficiency relative to the prior model (Table 5). Unlike for the set of calibration sites, there was no difference in the improvement between the assimilation period and the subsequent two-year period, suggesting that the model improvement is of general nature. In other words, the short-term (1-2 years) prognostic capabilities of the model have been largely improved for a 2 years horizon after assimilating CO_2-observations, also at the evaluation locations.

Table 5. Performance of the prior and posterior models compared with atmospheric CO_2 for constraining and evaluation sites and for the assimilation period (2005 - 2009) and the hindcast period (2010/2011). Abbreviations are: Bias: Model - Observations, Corr: Correlation, RMSE: Root mean squared error, NSE: Nash Sutcliffe model efficiency.

	2005 - 2009				2010/2011			
	Corr	Bias	RMSE	NSE	Corr	Bias	RMSE	NSE
Stations acting as constraint								
PRIOR	0.95	0.64	2.60	0.68	0.93	4.85	5.22	-0.69
CO2alone	0.96	-0.05	1.32	0.92	0.93	0.10	1.47	0.87
FAPARalone	0.91	8.91	9.84	-3.63	0.91	18.21	18.35	-19.86
JOINT	0.96	-0.09	1.35	0.91	0.93	-0.16	1.48	0.87
Stations withheld from assimilation								
PRIOR	0.86	1.20	3.83	0.52	0.84	5.18	6.03	-0.61
CO2alone	0.89	0.25	2.54	0.79	0.89	0.19	2.19	0.79
FAPARalone	0.84	9.73	10.84	-2.87	0.86	18.89	19.12	-15.14
JOINT	0.88	0.24	2.61	0.78	0.88	-0.05	2.28	0.77

4.3.1 Changes in Carbon fluxes causing the changes in simulated CO_2

The changes in simulated atmospheric CO_2 mole fractions originate from substantial changes of the seasonal amplitude and overall strength of the net carbon fluxes simulated by of JSBACH. The application of the CO_2-constraint increased the global net biome production (NBP) from 1.0 PgCyr^{-1} in the prior model to 3.2 PgCyr^{-1} in the CO2alone and JOINT experiments. Conversely, using only TIP-FAPAR as a constrained decreased the NBP to -2.2 PgCyr^{-1}, in other words, turning the biosphere into a net source (Table 6), inconsistent with current understanding of the global carbon cycle (Le Quéré et al., 2015). Despite the similarity of the global NBP for the experiments with CO_2 as a constraint, the spatial patterns of the NBP are different between the CO2alone and JOINT experiments (Fig. 6). The net uptake in both experiments originates from boreal and tropical regions. However, while the JOINT experiment shows an uptake in the boreal regions of coniferous evergreen and coniferous deciduous dominated pixels, the net CO_2 uptake in the CO2alone experiment is more concentrated to the coniferous deciduous regions. These differences will be further discussed in Sect. 4.4.2.

While the atmospheric observations constrain the net land-atmosphere CO_2 flux, the MPI-CCDAS model parameters affect the gross-fluxes, and thus the changes in NBP are again the consequence of substantially altered gross fluxes and land carbon pools. The generally reduced foliar area directly leads to a reduced gross primary production (GPP) of the terrestrial biosphere (in all experiments). The changes to the photosynthetic capacity (f_{photos}) (Table 2) often further reduce the uptake, a factor which is most pronounced for crop and tropical evergreen PFTs (Table 6 and Table 2). The GPP reduction is strongest for the CO2alone experiment and weakest (but still very pronounced) for FAPARalone. Even though the globally integrated posterior GPP values were somewhat different, the relative latitudinal patterns were fairly similar to each other (Fig. 7), and the reduction occurred in all regions, predominantly in tropical forests and grass/crop dominated temperate and boreal zones (Table 2).

Since the net carbon fluxes in the FAPARalone experiment were not constrained by the atmospheric CO_2 observations, the assimilation did not adjust the ecosystem respiration to balance the reduced productivity induced from the altered FAPAR. In the JSBACH model, autotrophic respiration is estimated as a direct function of GPP and canopy integrated carboylation capacity (Eq. A17), and thus quickly adjusts to any changes in GPP, On the time scales of five years in this study, this decline was not sufficient to balance the reduced GPP. As a consequence, the net flux to the atmosphere increased leading to the overestimation of the growth rate of atmospheric CO_2. Application of the CO_2 constraint in the CO2alone and JOINT experiment forces ecosystem respiration to be further reduced to match the atmospheric signal. This additional reduction in ecosystem respiration is mainly driven by a reduction of the initial soil carbon pool (via the modifier f_{slow}) to 50% and 51% for the JOINT and CO2alone experiment, respectively, which reduces heterotrophic respiration (Table 6; see also discussion in Section 5.4).

4.4 Regional differences among the experiments

In the following, we focus on differences in the spatial patterns of the results obtained for tropical regions and the boreal zone to highlight the interplay between parameters in a global, multi-data stream application of the MPI-CCDAS either by compensating effects between different model processes within one PFT as occurring in the tropics (Sect. 4.4.1) or by compensations between different parts of the globe (Sect. 4.4.2).

Table 6. Global averages of selected carbon cycle components for the years 2005 to 2009 in $\mathrm{PgC\,yr^{-1}}$ for fluxes and PgC for stocks and comparison with other estimates. Ra: autotrophic respiration. Rh: heterotrophic respiration. Reco: ecosystem respiration. Vegetation carbon is made up of all carbon stored in the living parts of the vegetation (including above and belowground carbon of plants and woods.)

	PRIOR	CO2alone	FAPARalone	JOINT	Other estimates	Other CCDAS
NPP	65.5	40.9	53.5	45.6	$44-66^a$	40^g
Ra	86.1	57.6	67.8	65.7		
Rh	64.5	37.6	55.4	42.2		
Reco	150.6	95.2	123.2	107.9		
GPP	151.6	98.4	121.3	111.3	$119\pm6^b, 123\pm8^c$	$109-164^h$
NBP	1	3.2	-2.2	3.2	2.4 ± 0.8^d	
Soil Carbon	2649	1064.7	2187.1	1122.3	1343^e	
Vegetation Carbon	424	388.5	420.5	407.3	442 ± 146^f	
Litter Carbon	239.9	189.8	212.8	193.9		

[a]Cramer et al. (1999); Saugier and Roy (2001); [b]Jung et al. (2011); [c]Beer et al. (2010); [d]Le Quéré et al. (2015); [e]http://webarchive.iiasa.ac.at/Research/LUC/External-World-soil-database/HTML/; [f]Carvalhais et al. (2014); [g]Rayner et al. (2005); [h]Koffi et al. (2012)

4.4.1 Tropics

The modelled foliar area in the tropics (mainly the tropical evergreen tree PFT) was similar for the JOINT and FAPARalone experiments (Fig. 3), but smaller for CO2alone. The simulated GPP of the JOINT experiment (Fig. 7) was somewhat lower than in the FAPARalone experiment, but still substantially larger than that of the CO2alone experiment. Notwithstanding these differences, the simulated net land-atmosphere CO_2 exchange (Fig. 6) of the JOINT experiment was closer to the posterior estimate of CO2alone than to that of FAPARalone in terms of absolute values.This result was caused by compensating effects of the different observational constraints (Fig. 8 and Table 2): the phenological parameters, notably τ_w and Λ_{max}, were substantially different between the FAPARalone and JOINT experiment, yet their modelled foliar area was very similar (Fig. 3). The reason for this was that the photosynthesis parameter modifier f_{photos} was reduced strongly in the JOINT experiment, which also drives the smaller GPP (relative to FAPARalone). Through the effect of net photosynthesis on canopy conductance (Eq. A14), the potential transpiration rate (E_{pot}; Eq. A5) was strongly decreased. Together with the increase of τ_w (Eq. A5) in the JOINT experiment, the decline in E_{pot} had the same effect on the simulated phenology as the smaller parameter changes in the FAPARalone experiment. The lack of an FAPAR constraint in the CO2alone experiment allowed the assimilation to overly reduce the foliar area by increasing τ_w at the prior rate of photosynthesis and thus E_{pot} to satisfy the constraint by the atmospheric CO_2 observations. As a consequence, due to the water-cycle feedback, the modelled foliar area was clearly different between the JOINT and CO2alone experiments.

4.4.2 Boreal zones

The CO2alone and JOINT experiments showed similar global statistics when compared with atmospheric CO_2 observations (Table 5 and Fig. 4). Their global and hemispheric net carbon uptake was similar (Northern Hemisphere: 2.24/2.20 $\mathrm{PgC\,yr^{-1}}$; Southern Hemisphere: 0.98/0.98$\mathrm{PgC\,yr^{-1}}$), but their underlying spatial patterns were different, in particular in the boreal zone (Fig. 6). The entire boreal zone took up a large share of the global carbon sequestration in the JOINT experiment (0.88 $\mathrm{PgC\,yr^{-1}}$), especially in coniferous deciduous (CD) dominated regions of Eastern Siberia (0.30 $\mathrm{PgC\,yr^{-1}}$). The CO2alone experiment showed a similar net Carbon uptake in the boreal region, but the uptake in the CD dominated region was 0.16 $\mathrm{PgC\,yr^{-1}}$ stronger than in the JOINT experiment. This difference was mainly driven by larger foliar area and increased leaf-level productivity (parameter f_{photos}) of the CD PFT in the CO2alone experiment. In the same latitudinal band, coniferous evergreen trees showed reduced foliar area in the CO2alone experiment compared to the JOINT experiment, reducing the net uptake by 0.16 $\mathrm{PgC\,yr^{-1}}$, such that the differences in these regions cancel each other. These relatively small spatial differences do not prevent the posterior JOINT and CO2alone experiment from capturing the amplitude of the seasonal cycle at individual northern-most stations.

This largely increased sink in Eastern Siberia could be an artefact of the set-up used for the data assimilation in this study. No nearby atmospheric stations constrains the net carbon sink in this region adequately, and the CD PFT only occurs dominantly in this region. In consequence, the PFT's parameters can not be adequately constrained by carbon cycle observations from other parts of the globe. This relative scarceness of observations and independency of other

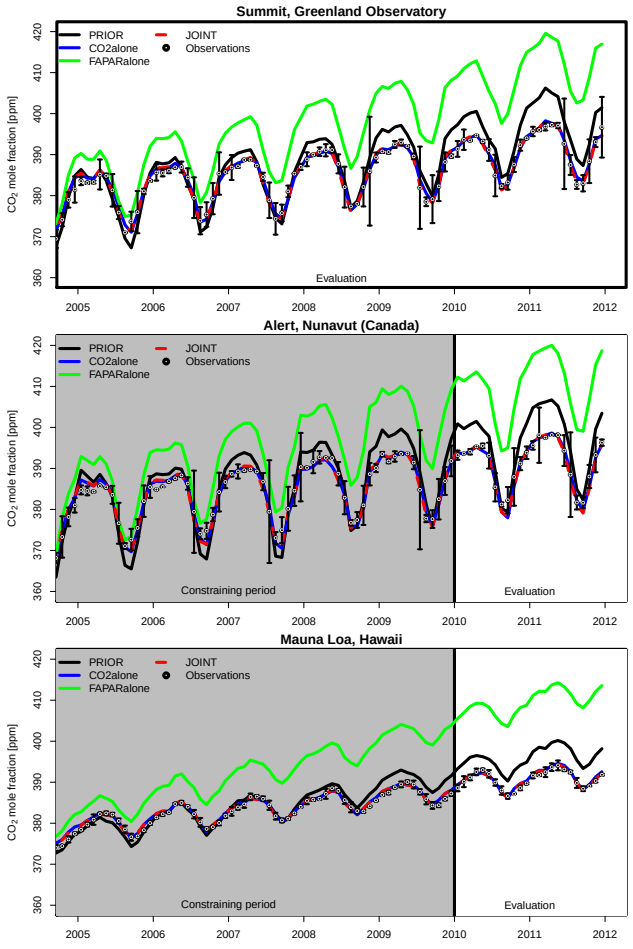

Figure 4. Time series of CO_2 as observed at the high latitude evaluation site Summit and at two constraining sites, one at high latitudes (Alert) and one representative for the Northern Hemisphere (Mauna Loa) for the different prior and posterior models. The observations are given together with their uncertainty.

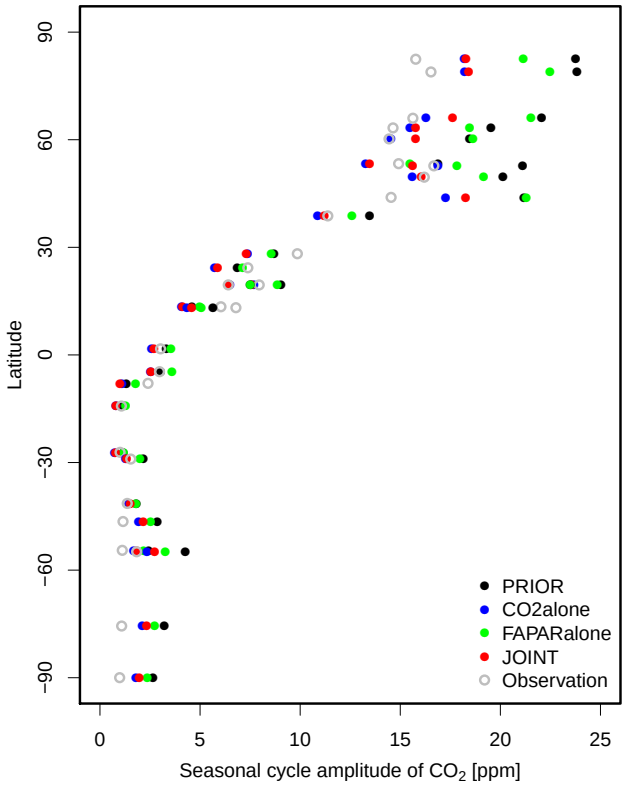

Figure 5. Latitudinal distribution of atmospheric CO_2 seasonal cycle amplitude, calculated as the difference between the maximum and minimum CO_2 mole fraction of the averaged seasonal cycle of the linearly de-trended signal from 2005 - 2009.

regions allows the East-Siberian net carbon uptake to compensate for other regions fluxes in order to match the global growth rate. Additional observations would be required to allow for spatially higher resolved estimation of the net fluxes.

5 Discussion

5.1 Comparison of the simulated Carbon cycle with independent estimates

We have demonstrated that the JSBACH model is capable of reproducing the seasonal cycle and five years trend of the observed atmospheric CO_2 (Fig.s 4 and 5 and Table 5). During the assimilation run, we have applied a careful selection of stations to avoid the impact of local sources on modelled atmospheric CO_2 mole fractions, which cannot be simulated with the current coarse resolution of the MPI-CCDAS. The evaluation at the cross-validation sites, which are located on land and thus closer to locally varying source patterns, also demonstrates a good skill of the posterior model for these sites. Overall, this does suggest that the improvement of the MPI-CCDAS's capability to capture the observed CO_2 dynamics at monthly to yearly time scales is reasonably robust. Our results further support earlier studies (Rayner et al., 1999; Kaminski et al., 1999; Peylin et al., 2013) that the observational network of atmospheric CO_2 only constrains a limited number of spatio-temporal flux patterns.

The application of the CCDAS led to significant changes of the modelled carbon cycle in JSBACH. The average global GPP of the JOINT experiment was substantially reduced from the prior run and was slightly lower than independent, data-driven estimates of $119 \pm 6\ \mathrm{PgC\,yr^{-1}}$ (Jung et al., 2011) and $123 \pm 8\ \mathrm{PgC\,yr^{-1}}$ (Beer et al., 2010), as well as estimates of comparable land surface models (ranging from 111 to 151 $\mathrm{PgC\,yr^{-1}}$; Piao et al. 2013). Partly driven by the reduction of GPP, the net primary production (NPP) was also significantly reduced to 46 $\mathrm{PgC\,yr^{-1}}$ in the JOINT experiment. While this is lower than the commonly accepted reference value of 60 $\mathrm{PgC\,yr^{-1}}$, it is still compatible with the range of available estimates for NPP of 44 - 66 $\mathrm{PgC\,yr^{-1}}$

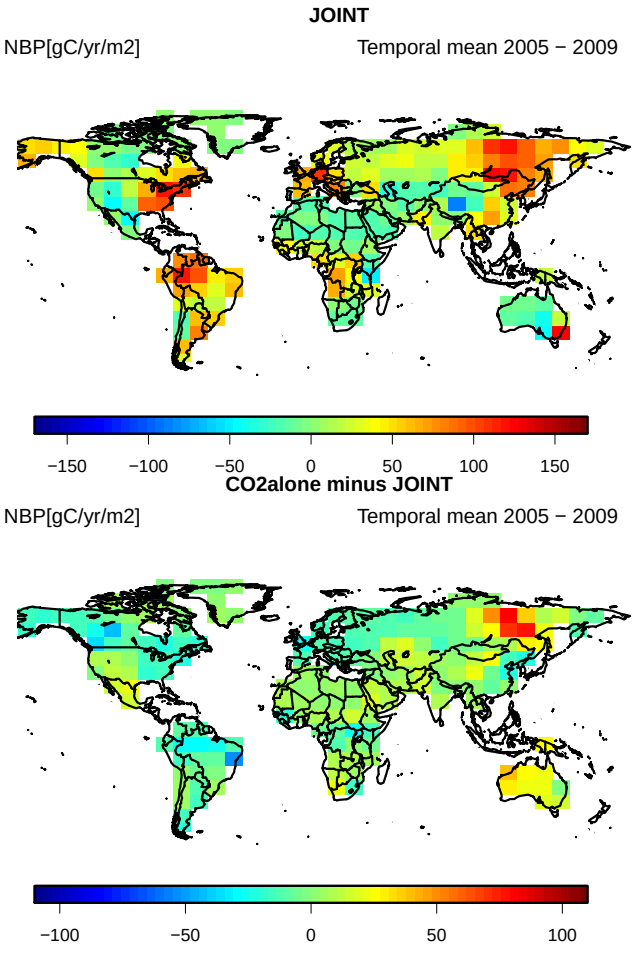

Figure 6. Temporally averaged NBP of the JOINT assimilation, differences of CO2alone to the JOINT experiment and the latitudinal distribution for the prior and posterior models.

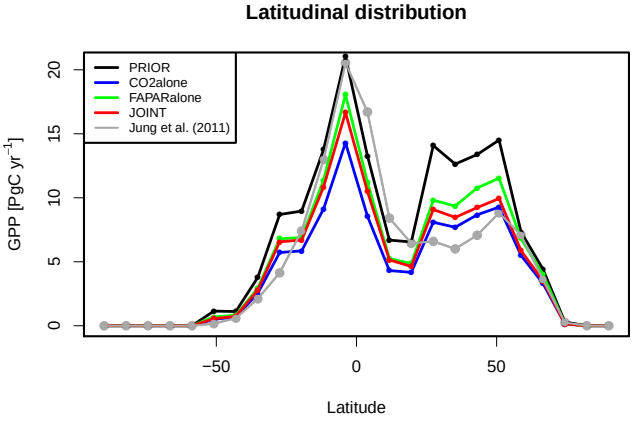

Figure 7. Latitudinal distribution of GPP for the prior and posterior models and comparison with the estimates of Jung et al. (2011).

(Cramer et al., 1999; Saugier and Roy, 2001). The latitudinal distribution of GPP in comparison to an empirical estimate based on satellite data and field measurements (Jung et al., 2011) shows that the global reduction of GPP leads to a better agreement of GPP in the northern extra-tropics between 30°N and 60°N, but to a lower GPP in the tropical rain forests (Fig. 7). The reduction of GPP in the northern extra-tropics is likely associated with the overestimation of the seasonal cycle of atmospheric CO_2 by the prior model, which was successfully reduced primarily by reducing northern extra-tropical productivity, in particular in temperate and boreal grasslands. Nevertheless, our study supports earlier findings that despite some constraint on northern extra-tropic production, the constraint of observed atmospheric CO_2 on global production is small (Koffi et al., 2012).

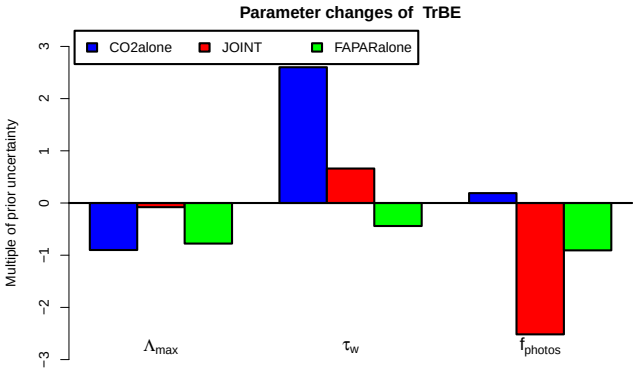

Figure 8. Parameter changes of tropical evergreen trees in multiples of the prior uncertainty (as $\frac{p_{po}-p_{pr}}{\sigma_{pr}}$).

A detailed comparison on the simulated vegetation and soil carbon stocks of the prior model is beyond the scope of this paper, partly because the simplifications of the spin-up procedure entail biases in predicted vegetation carbon stocks, as transient land-use changes and forest management, affecting forest age structure are ignored. It is nevertheless instructive to provide context for the simulated vegetation and soil carbon stocks by comparing them to the global totals of independent estimates. The posterior experiments showed only little less carbon in vegetation (389 - 420 PgC (composed of quickly overturning leaf and fine root carbon, as well as a woody carbon pool).) than the prior model (424 PgC). All of these estimates are lower than the 556 PgC vegetation carbon based on updated Olson's major world ecosystem carbon stocks[2], but comparable to a more recent estimate of global vegetation carbon storage of 442 ± 146 PgC (Carvalhais et al., 2014). The posterior amount of soil carbon from the assimilation runs using atmospheric CO_2 as a constraint compare favourably (within the uncertainty) to the estimates of 1343 PgC based on the Harmonized World Soil Database (HWSD)[3]. This estimate is more appropriate for the presented comparison than the more recent and higher estimate of soil carbon by Carvalhais et al. (2014) of 1836 -

[2]http://cdiac.ornl.gov/epubs/ndp/ndp017/ndp017b.html

[3]http://webarchive.iiasa.ac.at/Research/LUC/External-World-soil-database/HTML/

3257 PgC (95% confidence interval), as the latter includes estimates of permafrost carbon, which is not modelled with the current version of the MPI-CCDAS.

Our estimate of the net land carbon sink using atmospheric $\mathrm{CO_2}$ as a constraint is slightly larger than the residual land carbon sink estimate (without inclusion of land-use change fluxes) inferred from atmospheric measurements and auxiliary fluxes by Le Quéré et al. (2015), who derived a net uptake of $2.4 \pm 0.8\ \mathrm{PgC\,yr^{-1}}$ for the period 2000 - 2009. Correcting this estimate for the pre-industrial lateral carbon fluxes from land to the ocean via rivers would increase the terrestrial net land C uptake seen by the atmosphere (and thus the MPI-CCDAS) to $2.85\ \mathrm{PgC\,yr^{-1}}$; see Le Quéré et al. 2015 and Jacobson et al. 2007). Due to the interannual variability of the land sink, the shorter time-period of our sink estimate may have contributed to the difference between the estimates. More likely, one driving factor of our slightly larger estimate of the land net carbon uptake is from the comparatively small net ocean carbon uptake of $1.1\ \mathrm{PgC\,yr^{-1}}$ (Rödenbeck et al., 2013), which we prescribed in our assimilation. This compares to the estimate of $2.4 \pm 0.5\ \mathrm{PgC\,yr^{-1}}$ of Le Quéré et al. (2015). [4] (which reduces to $1.95\ \mathrm{PgC\,yr^{-1}}$ when correcting for the river input). Bearing in mind that the atmospheric $\mathrm{CO_2}$ observations more directly constrain the net land carbon fluxes at seasonal and annual scales than the gross fluxes or carbon pools, assuming a larger ocean net carbon flux would have reduced the land uptake. Explicitly accounting for DOC based carbon losses from land in the future will help to close the gap between the estimates, and thereby reduce the estimated land carbon storage inferred from the atmospheric data, and allow for the estimate of the MPI-CCDAS to be more compatible with the estimate of Le Quéré et al. (2015).

5.2 Comparison to previous studies

Our results are consistent with earlier studies, which showed that JSBACH overestimates the seasonal cycle amplitude of atmospheric $\mathrm{CO_2}$ (Dalmonech and Zaehle, 2013). The posterior estimates of this amplitude was considerably reduced and hence improved in all three experiments (Fig. 5). This also holds for FAPARalone, for which the comparison with $\mathrm{CO_2}$ is an independent evaluation. Note that the prior we reported here already relies on a corrected maximum leaf area index (Λ_{max}) of coniferous evergreen trees (see Sect. 3). For the run with the off-the-shelf configuration of JSBACH (results not shown), the high latitude mean seasonal cycle amplitude was clustered around 30 ppm, implying an overestimation of about 15 ppm. In the prior experiment, this overestimation was reduced to about 5 - 10 ppm, and further reduced in the FAPAR alone experiment (Fig. 5). In other words, boreal phenology considerably controls the seasonal cycle of the high latitude atmospheric $\mathrm{CO_2}$-signal and TIP-FAPAR can improve this aspect even though the $\mathrm{CO_2}$ trend is deteriorated (Fig. 4). Adding $\mathrm{CO_2}$ as a constraint further improves the fit to the seasonal cycle amplitude.

This conclusion is also supported by Kaminski et al. (2012), who constrained the BETHY-CCDAS jointly with atmospheric $\mathrm{CO_2}$ data and a different FAPAR product (Gobron et al., 2007). They found an improved seasonal cycle amplitude of $\mathrm{CO_2}$ for their joint assimilation with real data, which is in line with our findings. Through factorial uncertainty propagation with their assimilation scheme, Kaminski et al. (2012) also found that the inclusion of FAPAR yields only a moderate uncertainty reduction in the simulated carbon fluxes and mainly reduces the water flux uncertainties. Kaminski et al. (2012) therefore suggested that FAPAR only added little information to the modelled carbon cycle in addition to atmospheric $\mathrm{CO_2}$. In contrast, we have shown here a considerable impact of TIP-FAPAR by altering the spatial net Carbon flux patterns between the JOINT and CO2alone experiments.

Our study also showed a considerable difference of GPP estimates that are not likewise reflected in the net carbon fluxes, as these are more directly constrained by $\mathrm{CO_2}$. Also Koffi et al. (2012), using a variant of the BETHY-CCDAS (Rayner et al., 2005; Scholze et al., 2007), found large differences in their posterior GPP-estimates ranging from 109 - 164 $\mathrm{PgC\,yr^{-1}}$ when using different transport models, atmospheric station densities and prior uncertainties. As in our study, their relatively large GPP-ranges are not reflected in the net fluxes, as these are more directly constrained by the atmospheric $\mathrm{CO_2}$ network. A striking difference to the results of Koffi et al. (2012) occurs in the tropics, where they overestimate GPP compared to data-driven estimates, whereas the MPI-CCDAS underestimates GPP. As will be discussed later (Sect. 5.4), our underestimation of tropical GPP is likely a compensating effect arising from the respiration part of the model that only can be modified globally. This is not the case for the BETHY-CCDAS, which allows for a spatially more explicit control on heterotrophic respiration. It appears thus likely that a larger posterior GPP in the MPI-CCDAS could be expected with a system allowing for more spatial freedom in the respiration part of the assimilation system, for instance by making f_{aut_leaf} and f_{slow} vary by plant functional type. Regardless of this difference, our work further supports earlier findings (Rayner et al., 2005; Scholze et al., 2007; Koffi et al., 2012) that despite some constraint on northern extra-tropical GPP, the global land GPP cannot be well constrained with atmospheric $\mathrm{CO_2}$ alone. It appears thus vital that additional information is provided, especially in tropical regions, to further reduce uncertainty in the spatial distribution of the gross fluxes GPP and ecosystem respiration. This likely will propagate to an improved estimate of the net $\mathrm{CO_2}$-fluxes as well.

[4] The estimates of Rödenbeck et al. (2013) and Le Quéré et al. (2015) are not fully compatible because they differ in the accounting of carbon fluxes from rivers to the ocean.

5.3 Discussion of the assimilation procedure

The results clearly show that two data-streams can be successfully integrated with the MPI-CCDAS. The posterior parameter values (Table 2) were different between the FAPARalone and JOINT, as well as the CO2alone and JOINT experiments, showing that the joint use of the two data streams added information to the posterior parameter vector by preventing the degradation of the phenology simulation when trying to fit the CO_2 observations (Table 5 and 4). This is also supported by the fact that value of the cost function of the JOINT assimilation roughly equals the sum of the single data-stream experiments, indicating consistency of the model with both data streams.

Hence, although the JSBACH phenology is only weakly influenced by the carbon cycle component of JSBACH and mainly controlled by other drives (e.g.: soil moisture, temperature), there are strong interactions among carbon and water cycle parameters and simulated FAPAR, a finding supported by Forkel et al. (2014). Thus the combination of different data streams in the JOINT experiment helped estimating parameters of different processes to remain within acceptable bounds. The capability of assimilating multiple data streams simultaneously is a distinct advantage of the MPI-CCDAS over alternative strategies that assimilate multiple data streams by following a sequential design of assimilating FAPAR prior to carbon cycle information. An implementation of such a sequential assimilation likely reduces the number of parameters to be optimized in each step, and therefore allows a quicker solution of the optimisation problem. However, this advantage comes with the cost of breaking the linkage between parameters which can lead to situations, where the posteriori results of a sequential assimilation experiment will not match the observations equally well as with a simultaneous assimilation. Since our results have demonstrated that a joint assimilation is feasible without impairing the fit to the individual data sources, a joint assimilation approach appears therefore recommendable.

The assimilation procedure achieved a strong reduction of the cost function and the norm of the gradient (see Table 3). Although the relative reduction in the norm of the gradient was larger in the CO_2-cases than in the FAPARalone case, the norm did not not approach zero - contrary to the FAPARalone case. Such a non-zero gradient was also noted by Rayner et al. (2005) in their CO_2 assimilation with the BETHY-CCDAS. The fact that the MPI-CCDAS successfully reduces the norm of the gradient for FAPAR suggests that this is not a general failure of the MPI-CCDAS, but specific to the particularities of the CO_2 set-up. It is presently unclear, what is causing the assimilation to fail to reach the minimum of the cost function. Investigation of the non-linear nature and potential numerical issues regarding the computation of the gradient $\frac{\partial J}{\partial p}$ (Eq. 1) might be needed. Further tests with alternative station network settings, parameter priors or time-periods will provide more insight into approaches to tackle this issue. Nevertheless, we believe that our results can still be meaningfully interpreted and used to evaluate the general capacity of the MPI-CCDAS as a comprehensive data assimilation tool.

5.4 Comments on the parameter set-up

The results presented in 4.2 show, that there is a certain degree of equifinality in the parameter values obtained from the assimilation of TIP-FAPAR, as the combination of different parameter values can lead to fairly similar results. This can happen when (i) certain parameters enter an insensitive regime where parameter differences do hardly propagate to differences in the modelled foliar area, (ii) pixels are a composite of different plant functional types that can show compensating effects, and (iii) the CO_2 constraint may still impose an additional weight on changing FAPAR because of the feedbacks on photosynthesis.

Another cautionary note about the posterior parameter values is warranted: Some of the parameters of the JOINT and CO2alone experiment were altered strongly compared to the assumed prior uncertainty. This is possible within the MPI-CCDAS, because the prior contribution to the cost-function is weak due to the small number of parameters compared to the number of observations. One example is the f_{slow} parameter, which controls the initial soil Carbon pool size and thus the disequilibrium between GPP and respiration (Table 2). Another example is the photosynthesis parameter f_{photos} for the tropical evergreen PFT in the JOINT experiment, which was reduced by more than 2.5 times the prior uncertainty and to roughly 75% of its prior value. As a consequence, the assimilation procedure can result in parameter values with small prior probabilities. This either points toward too tight prior uncertainties or to model structural problems.

One such structural problem may be that the current MPI-CCDAS excludes the model spin-up from the assimilation procedure for reasons of computational efficiency: the solution applied was to allow the MPI-CCDAS to manipulate the initial soil carbon pool by one globally valid modifier. This choice was made because allowing to control the spatial structure of the carbon pools would require several more parameters to be optimized, which would very likely suffer from a strong equifinality problem, and which would considerably extend the already lengthy run-time of the MPI-CCDAS. Our results demonstrate that this spin-up approach allows to adequately reproduce the space-time structure of the atmospheric CO_2 budget at the time scale of several years (Fig. 4 and Table 5). However, this approach likely introduces an imprint of the spatial distribution of the prior productivity on the final model outcome, which may cause imperfections in the ability of the MPI-CCDAS to accurately capture the spatial distribution of the net land carbon uptake, and in turn also affect the posteriori parameter vector. Allowing for more spatially explicit modifiers for the initial carbon pools (as is done in the BETHY-CCDAS) by e.g. linking the

initial soil disequilibrium to a particular PFT, would be a first step forward.

The stiffness of the MPI-CCDAS respiration parametrisation (with only a few adjustable parameters) likely also caused the reduction of temperate GPP to propagate into the tropical zone, leading to the strong change of f_{photos} for the tropical evergreen PFT in the JOINT experiment. Because the overall net CO_2 flux is constrained by the atmospheric observations, reduction in temperate GPP requires a corresponding adjustment of the ecosystem respiration to balance the budget. While lowering GPP also reduces autotrophic respiration (Eq. A17), any further reduction in respiration in the temperate zone by adjusting autotrophic (f_{aut_leaf}) or heterotrophic respiration parameters (Q_{10}, f_{slow}) would also affect tropical respiration, because in the current version of the MPI-CCDAS these parameters are assumed to be valid globally. To balance the budget, a reduction in tropical GPP might have been required. Because of enough water availability in the tropics a phase-shift in the dry-wet cycle in the Amazonian rain forest may play a minor role in the down-regulation of GPP during the assimilation. At least no phase mismatch in atmospheric CO_2 is observed at Mauna Loa (Fig. 4) that would suggest such a problem.

5.5 Further development of the MPI-CCDAS

The application of the MPI-CCDAS allows to detect model structural errors and/or deficits in the set-up, which then can lead to a reformulation of the forward model (see e.g.: Kaminski et al., 2003; Rayner et al., 2005; Williams et al., 2009; Kaminski et al., 2013). The framework described here can be steadily improved through regular improvements of the JSBACH model structure by including missing or correcting false model parametrisations (e.g. Knauer et al., 2015). The system is also versatile enough to add more constraints from relevant and complementary, multiple data sources (Luo et al., 2012) to come up with more robust regional estimates than the current atmospheric inversion allow. Beside the previously discussed limitation related to the spin-up and the representation of initial carbon pools, we can suggest also other analysis and system developments to further improve the MPI-CCDAS.

The discrepancies between FAPARalone and JOINT in the foliar area estimates for crop-dominated regions, even though large in extent, originates from the exclusion of TIP-FAPAR as constraint for these regions. This likewise affected the extra-tropical deciduous PFT, that co-occurred dominantly in the same pixels. Increasing the constraining power of TIP-FAPAR by either adding more pixels as constraints or by increasing the resolution to finer grids might further improve the phenology. In this context we note that the per-pixel uncertainty ranges in the TIP-FAPAR product also reflect limitations of the information content that can be derived from sunlight reflected to space in the optical domain (i.e. the input to TIP) in particular over dense canopies. Formal uncertainty propagation can quantify the information content in the FAPAR product on gross-fluxes or, conversely, derive accuracy requirments for optical products (Kaminski et al., 2012).

We demonstrated the value of using a CCDAS instead of a pure atmospheric inversion to estimate the land net carbon flux, because the CCDAS can ingest complementary data streams, which may help to further constrain the regional estimates of the net land carbon flux. In this first version of the MPI-CCDAS, we have assumed the net fluxes other than those simulated with JSBACH (i.e. fossil fuel emissions and ocean exchange), as well as the atmospheric drivers to JSBACH to be perfectly known, and thus impute all the model-data mismatch on shortcomings of the land-surface model. It would be desirable to also account for the uncertainties in these components of the modelling system to more robustly identify potential model shortcomings. Further assessing the relative importance of different error sources (e.g. in the land cover type parameterization, model biases or observational errors) with a system such as the MPI-CCDAS would allow to highlight priority areas to reduce their uncertainties and further constrain the global carbon cycle numbers as given in table 6

Our results show that applying FAPAR and atmospheric CO_2 as a constraint for the JSBACH model leads to an improved simulation of phenology and northern extra-tropical GPP. As a consequence of the assimilation procedure, the model also captures the magnitude of the global and hemispheric net biome exchange. This is a major step forward to including better constrained terrestrial models for the estimation of the global carbon budget (Le Quéré et al., 2015). However, we have set up the model such that it attributes the difference between prior and posterior sink (i.e. 2.2 PgCyr^{-1}) to the soil carbon storage. It has been long known that the terrestrial net carbon uptake, and thus the CO_2 signal seen by the atmospheric observations, is strongly affected by natural (such as fire) and anthropogenic disturbances (such as land-use change; Houghton et al. 2012). These processes contribute to the disequilibrium of vegetation and soil carbon pools with vegetation production, and thus affect the spatial pattern of terrestrial carbon release and uptake. Without consideration of these processes, one should be careful in analysing the MPI-CCDAS projected carbon cycle trends and attribution of drivers of the trends. The tangent-linear version of the JSBACH model contained in the MPI-CCDAS already has the appropriate modules to simulate disturbance by fire (Lasslop et al., 2014) and land-use (Reick et al., 2013). A further development of the MPI-CCDAS could be to activate these processes. In order to improve on the current situation it might also be desirable to constrain the post-disturbance dynamics of the carbon pools or at least to analyse how well these are constrained. This would also allow to add more data streams to potentially disentangle the tight parameter linkages in the model.

6 Conclusions

The assimilation of five years of remotely sensed FAPAR and atmospheric CO_2 observations with the MPI-CCDAS was generally successful in that the fairly substantial model-data mismatch of the prior model was largely reduced. The assimilation procedure strongly reduced the too large prior-estimate of GPP, and generally led to an improvement of the simulated carbon cycle and its seasonality. The resultant carbon cycle estimates compared favourably to independent data-driven estimates, although tropical productivity was lower than these estimates. The posterior global net land-atmosphere flux was well constrained and commensurate with independent estimates of the global carbon budget. Our analysis of the prognostic fluxes for a consecutive 2-year period as well as at stations withheld from the assimilation procedure demonstrates that our results are robust.

The factorial inclusion of FAPAR and atmospheric CO_2 as a constraint clearly demonstrated that the two data streams can be simultaneously integrated with the MPI-CCDAS. We have shown the potential of multiple-data-stream assimilation by adding TIP-FAPAR as a constraint and have shown how this data stream helps constraining the foliar area without degrading the ability of the model to capture seasonal and yearly dynamics of the atmospheric CO_2 mole fractions. However, the multi-data assimilation also pointed to model structural problems in the initialisation, which need to be addressed. Nevertheless, our study highlights the potential of adding new data streams to constrain different processes in a global ecosystem model.

This study thus provides an important step forward in the development of global atmospheric inversion schemes. Adding a process-based component, belonging to a coupled carbon-cycle climate model, allows to disentangle the drivers of the terrestrial carbon balance. It also gives the opportunity to apply multiple data streams to constrain these drivers. On the one hand improving the assimilation system and on the other hand adding more data streams can ultimately lead to regionally constrained estimates of the terrestrial carbon balance for the assessment of current and future trends.

Code availability

The JSBACH model code is available upon request to S. Zaehle (soenke.zaehle@bgc-jena.mpg.de)

The TM3 model code is available upon request to to C. Rödenbeck (christian.roedenbeck@bgc-jena.mpg.de)

The TAF generated derivative code is subject to license restrictions and not available.

Appendix A: Model description of JSBACH

A1 The phenology module

In the revised MPI-CCDAS phenology scheme (Knorr et al., 2010), each plant functional type is assigned to a specific phenotype, implying limitations on phenology by water (tropical and raingreen PFTs), water and temperature (herbaceous PFTs) and temperature and daylight (extra-tropical tree PFTs; see Table 1). The evolution of the leaf area index Λ (LAI) on a daily time-step Δt is described as

$$\Lambda(t+\Delta t) = \Lambda_{lim} - [\Lambda_{lim} - \Lambda(t)]e^{-r\Delta t} \quad \text{(A1)}$$

with the inverse time scale r, which is defined as:

$$r = \xi f + (1-f)/\tau_l \quad \text{(A2)}$$

The parameter ξ describes the rate of initial leaf growth, and the parameter τ_l describes how quickly leafs are shed. f specifies the stage of the vegetation being fully active at $f = 1$ or fully dormant at $f = 0$ (see Eq. A4). Λ_{lim} is defined as:

$$\Lambda_{lim} = \xi \Lambda_{max} f/r \quad \text{(A3)}$$

where the parameter Λ_{max} is the maximum allowed LAI.

The scheme accounts for naturally occuring heterogeneity within the area of a model grid-cell by smoothly varying the vegetation's state f between the two extremes. The transition is controlled either by the length of the day t_d or a temporally averaged temperature T_m with exponentially decaying weights for older periods with a time scale of 30 days (for details see Knorr et al. (2010)).

$$f = \Phi\left(\frac{T_m - T_\phi}{T_r}\right)\Phi\left(\frac{t_d - t_c}{t_r}\right) \quad \text{(A4)}$$

with the temperature control parameters T_ϕ, T_r and day-length control parameters t_c and t_r and the cumulative normal distribution Φ (with mean T_m resp. t_d and standard deviation T_r resp. t_r).

Water limitation is incorporated by calculating a water-limited maximum leaf area index Λ_W that cannot be exceeded by the actual LAI:

$$\Lambda_W = \frac{W\Lambda^{last}}{E_{pot}\tau_W} \quad \text{(A5)}$$

with a water limitation time scale τ_W. The potential evaporation E_{pot}, the relative root-zone moisture W and the LAI Λ^{last} are taken from the previous day averages. Λ_W itself is a temporally averaged LAI with exponentially decaying weigths of 30 day time-scale, similar to temperature and day length above.

A2 Photosynthesis

Photosynthesis in JSBACH follows Farquhar et al. (1980) for C3-plants and Collatz et al. (1992) for C4- plants, with details as described in Knorr and Heimann (2001) and Knorr

(1997). Net leaf CO_2 uptake is the minimum of a carboxylation limited photosynthesis rate J_C and of electron transport limited rate J_E minus dark respiration R_d:

$$A = \min(J_C, J_E) - R_d \tag{A6}$$

The carboxylation limited rate is calculated as:

$$J_C = V_m \frac{C_i - \Gamma_\star}{C_i + K_C(1 + O_x/K_O)} \tag{A7}$$

with the leaf internal CO_2-Concentration C_i, the oxygen concentration O_x (0.21 mol/mol) and the CO_2 compensation point (without dark respiration) $\Gamma_\star = 1.7\mu\text{mol/mol}^\circ\text{C} \cdot T$ which depends on temperature T (in °C). K_C and K_O are the Michealis-Menten constants for CO_2 and O_2 and V_m is the maximum carboxylation rate. The latter three all depend on the canopy temperature T_c (in K) in the form (exemplified by V_m):

$$V_m = Vc_{max} \cdot \exp(\frac{E_V T_0}{T_1 R_g T_c}) \tag{A8}$$

with activation energy $E_V = 58520$ Jmol^{-1} and gas constant $R_g = 8.314$ JK^{-1}mol^{-1}. $T_1 = 298.16$ °C is a reference temperature and $T_0 = T_c - T_1$ the difference to this reference. Vc_{max} is the maximal carboxylation rate at 25 °C and is given in Table D1. Temperature dependence of K_C and K_O are calculated with a similar approach with reference values at 25 °C for $K_{C0} = 460 \cdot 10^{-6}$ mol/mol and $K_{O0} = 330 \cdot 10^{-3}$ mol/mol and activation energies of $E_C = 59356$ Jmol^{-1} and $E_O = 35948$ Jmol^{-1}, respectively.

The electron transport limited rate, J_E, is calculated as

$$J_E = J \frac{C_i - \Gamma_\star}{4(C_i - 2\Gamma_\star)} \tag{A9}$$

with the photon capture efficiency $\alpha = 0.28$ mol(electrons)/mol(photons), the absorption rate of photosynthetically active radiation I, and with

$$J = \frac{\alpha I J_m}{\sqrt{J_m^2 + \alpha^2 I^2}}. \tag{A10}$$

The limiting rate constant J_m depends on the temperature with a maximum rate of electron transport J_{max} at 25 °C (Table D1):

$$J_m = J_{max} \cdot T/25°C \tag{A11}$$

Photosynthesis for C4-plants follows Collatz et al. (1992) and is the minimum among the three limiting rates $J_e = V_m$, $J_c = kC_i$ and $J_i = \alpha_i I$ with the quantum efficiency $\alpha_i = 0.04$ and k:

$$k = J_{max} \cdot 10^3 \exp(\frac{E_K T_0}{T_1 R_g T_c}) \tag{A12}$$

with $E_K = 50967$ Jmol^{-1}.

Dark respiration is modelled depending on Vc_{max} according to

$$R_d = fr_{C3|C4} Vc_{max} \cdot \exp(\frac{E_R T_0}{T_1 R_g T_c}) \tag{A13}$$

with activation energy $E_R = 45000$ Jmol^{-1}, and $fr_{C3|C4} = 0.011|0.031$ for C3 and C4 plants, respectively. Dark respiration is reduced to 50% of its value during light conditions (Brooks and Farquhar, 1985).

Photosynthesis and dark respiration are inhibited above 55°C. Calculations are performed per PFT and three distinct canopy layers, which vary in depth according to the current leaf area index, assuming that within the canopy nitrogen, and thus Vc_{max}, J_{max}, and R_d decline proportionally with light levels in the canopy. GPP values per PFT are integrated to grid-cell averages according to the cover fractions of each PFT within each grid-cell.

A3 Carbon-water coupling

JSBACH employs a two-step approach to couple the plant carbon and water fluxes (Knauer et al., 2015). Given a photosynthetic-pathway dependent specific maximal internal leaf CO_2 concentration (C_i), a maximal estimate of stomatal conductance (gs_{pot}) is derived for each canopy layer, which is then reduced by a water-stress factor (w_s) to arrive at the actual stomatal conductance (gs_{act}) (see Knorr, 1997, 2000, and references therein).

$$gs_{act} = w_s \cdot gs_{pot} = w_s \cdot 1.6 \cdot \frac{A}{C_a - C_i} \tag{A14}$$

where C_a and C_i are the external and internal leaf CO_2 concentrations. The water-stress factor w_s is defined as

$$w_s = \min(\frac{W_{root} - W_{wilt}}{W_{crit} - W_{wilt}}, 1) \tag{A15}$$

where W_{root} is the actual soil-moisture in the root zone, and $W_{crit|wilt}$ define the soil moisture levels at which stomata begin to close, or reach full closure, respectively. Soil moisture and bare soil evaporation are calculated according to the multi-layer soil water scheme of Hagemann and Stacke (2014).

Given the water-stressed stomatal conductance, leaf internal CO_2 concentration and carbon assimilation are then recalculated for each canopy layer by solving simultaneously the diffusion equation (Eq. A14) and the photosynthesis equations as outlined above (Sec. A2)

A4 Land carbon pools, respiration and turnover

The vegetation's net primary production (NPP) is related to the net assimilation (A) as

$$NPP = A - R_m - R_g \tag{A16}$$

where R_g is the growth respiration, which is assumed to be a fixed fraction (20%) of $A - R_m$. R_m is the maintenance respiration, which is assumed to be coordinated with foliar photosynthetic activity, and thus scaled to leaf dark respiration via f_{aut_leaf} (Knorr, 2000)

$$R_m = \frac{R_d}{f_{aut\_leaf}} \tag{A17}$$

with the dark respiration R_d as given in Eq. A13. As a consequence, an increase in f_aut_leaf leads to an increase in NPP.

NPP is allocated to either a green or woody pool given fixed, PFT-specific allocation constants. The green pool turns to litter according to the leaf phenology, whereas the woody turnover rate is prescribed as a fixed constant.

JSBACH considers three litter pools (above ground green, below ground green and woody) with distinct, PFT-specific turnover times, as well as a soil organic matter pool with a longer turnover time. Heterotrophic respiration for each of these pools responds to temperature according to a Q_{10} formulation:

$$R_{pool} = \alpha_{resp} Q_{10}^{(T-T_{ref})/10} / \tau_{pool} \cdot C_{pool} \tag{A18}$$

with a soil-moisture dependent factor $0 <= \alpha_{resp} <= 1$. C_{pool} is either the slow soil carbon pool, above or below ground green litter or wood litter pool and T is temperature and $T_{ref} = 0°\mathrm{C}$ the reference temperature and a pool depended turnover rate τ_{pool} (more details on the carbon balance sub-module can be found in Goll et al., 2012).

Appendix B: CO_2 station list

The stations of atmospheric CO_2-observations used for assimilation and evaluation are given in Table B1 resp. Table B2.

Appendix C: Mapping variants

For performance reasons, the assimilation is not performed in the physical parameter space but parameters p are transformed to x expressed in multiples of the prior uncertainty, the intrinsic units of the problem (Kaminski et al., 1999). The most basic mapping is:

$$x = \frac{p - p_0}{\sigma_{prior}} \qquad \Leftrightarrow \qquad p = p_0 + x\sigma_{prior} \tag{C1}$$

Table B1. CO_2 stations used in the assimilation together with their median uncertainty.

ID	Longitude	Latitude	Median Uncertainty
MNM	153.97	24.30	1.4
SBL	-60.02	43.93	5.9
ALT	-62.52	82.45	1.8
ASC	-14.42	-7.92	1.1
AZR	-27.19	38.76	1.9
BHD	174.90	-41.40	1.0
CHR	-157.17	1.70	1.0
CRZ	51.85	-46.45	1.0
EIC	-109.45	-27.15	1.1
ESP	-126.83	49.56	2.9
GMI	144.78	13.43	1.2
HBA	-26.65	-75.58	1.0
ICE	-20.21	63.30	1.9
KER	-177.15	-29.03	1.0
KUM	-154.82	19.52	1.6
MHD	-9.90	53.33	2.4
MID	-177.37	28.22	1.7
MQA	158.97	-54.48	1.0
RPB	-59.43	13.17	1.1
SEY	55.17	-4.67	1.0
SHM	174.10	52.72	2.1
SIS	-1.23	60.23	3.1
STM	2.00	66.00	3.2
TDF	-68.48	-54.87	1.0
ZEP	11.88	78.90	2.3
MLO	-155.58	19.53	1.1
SMO	-170.57	-14.25	1.0
SPO	-24.80	-89.98	1.0

An extension of this is to apply lower bounds in the mapping back to physical space with

$$p = p_{min} + x_{low}/x\sigma_{prior}$$
only if
$$x < x_{low} = \frac{p_{min} + \sigma_{prior} - p_0}{\sigma_{prior}} \tag{C2}$$

with p_{min} the minimum allowed parameter value.

Appendix D: Parameter values

Some parameters were modified with a factor within the MPI-CCDAS, because model structure did not allow to directly change these values and thus such an approach was required. The parameter values are listed in Table D1.

Table B2. CO_2 stations used for evaluation that have not been used as constraints for the assimilation.

ID	Longitude	Latitude
PAL	24.12	67.97
PRS	7.70	45.93
RYO	141.83	39.03
YON	123.02	24.47
CBA	-162.72	55.20
CFA	147.06	-19.28
CGO	144.70	-40.68
COI	145.50	43.15
CYA	110.52	-66.28
HAT	123.80	24.05
IZO	-16.48	28.30
KEY	-80.20	25.67
LEF	-90.27	45.93
LJO	-117.25	32.87
LMP	12.61	35.51
MAA	62.87	-67.62
NWR	-105.60	40.05
PSA	-64.00	-64.92
SUM	-38.47	72.57
TAP	126.13	36.73
UTA	-113.72	39.90
UUM	111.10	44.45
WIS	34.88	31.13
WLG	100.91	36.28
BRW	-156.60	71.32
SYO	39.58	-69.00
CMN	10.70	44.18
SCH	7.92	47.92

Appendix E: PFT-distribution

The vegetation distribution of the PFT's as prescribed in the MPI-CCDAS is given in Fig. E1.

Table D1. Values of those parameters that have been changed with a multiplicative factor during the assimilation.

PFT	TrBE	TrBD	ETD	CE	CD	RS	TeH	TeCr	TrH	TrCr
Prior Λ_{max} [m^2/m^2]	7.0	7.0	5.0	1.7	5.0	2.0	3.0	4.0	3.0	4.0
Joint Λ_{max} [m^2/m^2]	6.9	4.1	4.9	1.7	3.2	2.7	1.9	2.5	1.6	2.1
Prior Vc_{max} [$\mu mol/m^2 s$]	39.0	31.0	66.0	62.5	39.1	61.7	78.2	100.7	8.0	39.0
Joint Vc_{max} [$\mu mol/m^2 s$]	29.2	33.3	65.1	59.2	40.6	62.1	75.4	67.9	8.3	34.1
Prior J_{max} [$\mu mol/m^2 s$]	74.1	58.9	125.4	118.8	74.3	117.2	148.6	191.3	140.0	700.0
Joint J_{max} [$\mu mol/m^2 s$]	55.5	63.3	123.7	112.5	77.2	117.9	143.2	129.0	145.0	611.2

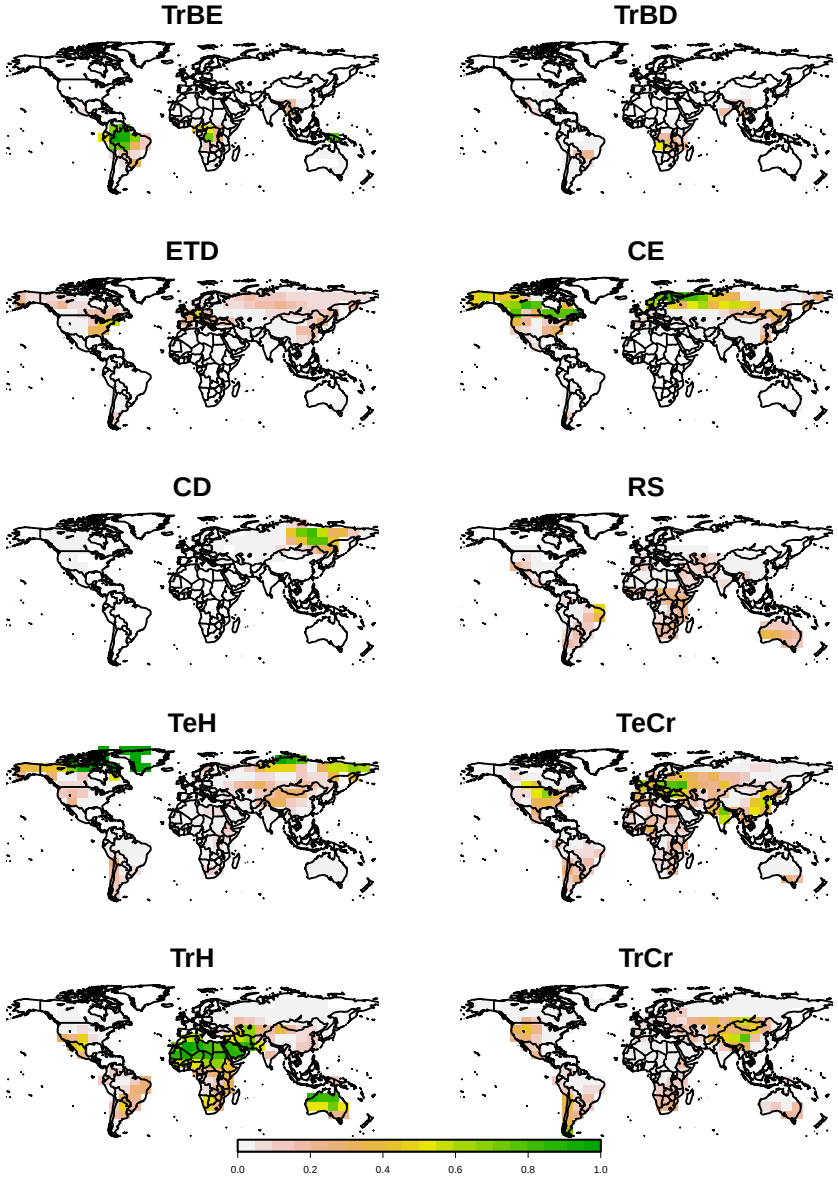

Figure E1. Fractional vegetation coverage of the PFT's as prescribed in the MPI-CCDAS. See Table 1 for abbreviations.

Acknowledgements. The research leading to this publication was supported by the European Space Agency through the STSE Carbonflux (contract no. 4000107086/12/NL/Fv0), the European Community within its 7th framework programme under contract number (GEOCARBON; FP7-283080), as well as the Max Planck Society for the Advancement of Science, e.V. through the ENIGMA project. The authors thank P. Peylin for providing the fossil fuel emission data, M. Scholze, W. Knorr and K. Scipal for fruitful discussions and C. Reick, R. Schnur and V. Gayler for assistance with the JSBACH model.

References

Anav, A., Friedlingstein, P., Kidston, M., Bopp, L., Ciais, P., Cox, P., Jones, C., Jung, M., Myneni, R., and Zhu, Z.: Evaluating the Land and Ocean Components of the Global Carbon Cycle in the CMIP5 Earth System Models, J. Climate, 26, 6801–6843, 2013.

Bacour, C., Peylin, P., MacBean, N., Rayner, P. J., Delage, F., Chevallier, F., Weiss, M., Demarty, J., Santaren, D., Baret, F., Berveiller, D., Dufrêne, E., and Prunet, P.: Joint assimilation of eddy covariance flux measurements and FAPAR products over temperate forests within a process-oriented biosphere model, Journal of Geophysical Research: Biogeosciences, 120, 1839–1857, doi:10.1002/2015JG002966, http://dx.doi.org/10.1002/2015JG002966, 2015JG002966, 2015.

Beer, C., Reichstein, M., Tomelleri, E., Ciais, P., Jung, M., Carvalhais, N., Rödenbeck, C., Arain, M. A., Baldocchi, D., Bonan, G. B., Bondeau, A., Cescatti, A., Lasslop, G., Lindroth, A., Lomas, M., Luyssaert, S., Margolis, H., Oleson, K. W., Roupsard, O., Veenendaal, E., Viovy, N., Williams, C., Woodward, F. I., and Papale, D.: Terrestrial Gross Carbon Dioxide Uptake: Global Distribution and Covariation with Climate, Science, 329, 834–838, doi:10.1126/science.1184984, 2010.

Booth, B. B. B., Jones, C. D., Collins, M., Totterdell, I. J., Cox, P. M., Sitch, S., Huntingford, C., Betts, R. A., Harris, G. R., and Lloyd, J.: High sensitivity of future global warming to land carbon cycle processes, Environmental Research Letters, 7, 024 002, 2012.

Brooks, A. and Farquhar, G.: Effect of temperature on the CO2/O2 specificity of ribulose-1,5-bisphosphate carboxylase/oxygenase and the rate of respiration in the light, Planta, 165, 397–406, doi:10.1007/BF00392238, 1985.

Brovkin, V., Raddatz, T., Reick, C. H., Claussen, M., and Gayler, V.: Global biogeophysical interactions between forest and climate, Geophysical Research Letters, 36, doi:10.1029/2009GL037543, 2009.

Carvalhais, N., Reichstein, M., Seixas, J., Collatz, G. J., Pereira, J. S., Berbigier, P., Carrara, A., Granier, A., Montagnani, L., Papale, D., Rambal, S., Sanz, M. J., and Valentini, R.: Implications of the carbon cycle steady state assumption for biogeochemical modeling performance and inverse parameter retrieval, Global Biogeochemical Cycles, 22, n/a–n/a, doi:10.1029/2007GB003033, http://dx.doi.org/10.1029/2007GB003033, gB2007, 2008.

Carvalhais, N., Forkel, M., Khomik, M., Bellarby, J., Jung, M., Migliavacca, M., Mu, M., Saatchi, S., Santoro, M., Thurner, M., Weber, U., Ahrens, B., Beer, C., Cescatti, A., Randerson, J. T., and Reichstein, M.: Global covariation of carbon turnover times with climate in terrestrial ecosystems, Nature, 514, 213–217, 2014.

Clerici, M., Vossbeck, M., Pinty, B., Kaminski, T., Taberner, M., Lavergne, T., and Andredakis, I.: Consolidating the Two-Stream Inversion Package (JRC-TIP) to Retrieve Land Surface Parameters From Albedo Products, Selected Topics in Applied Earth Observations and Remote Sensing, IEEE Journal of, 3, 286–295, doi:10.1109/JSTARS.2010.2046626, 2010.

Collatz, G., Ribas-Carbo, M., and Berry, J.: Coupled Photosynthesis-Stomatal Conductance Model for Leaves of C_4 Plants, Functional Plant Biol., 19, 519–538, 1992.

Conway, T. J., Tans, P. P., Waterman, L. S., Thoning, K. W., Kitzis, D. R., Masarie, K. A., and Zhang, N.: Evidence for interannual variability of the carbon cycle from the National Oceanic and Atmospheric Administration/Climate Monitoring and Diagnostics Laboratory Global Air Sampling Network, Journal of Geophysical Research: Atmospheres, 99, 22 831–22 855, doi:10.1029/94JD01951, 1994.

Cramer, W., Kicklighter, D. W., Bondeau, A., Iii, B. M., Churkina, G., Nemry, B., Ruimy, A., Schloss, A. L., and Intercomparison, T. P. O. T. P. N. M.: Comparing global models of terrestrial net primary productivity (NPP): overview and key results, Global Change Biology, 5, 1–15, doi:10.1046/j.1365-2486.1999.00009.x, 1999.

Dalmonech, D. and Zaehle, S.: Towards a more objective evaluation of modelled land-carbon trends using atmospheric CO_2 and satellite-based vegetation activity observations, Biogeosciences, 10, 4189–4210, doi:10.5194/bg-10-4189-2013, 2013.

Dalmonech, D., Zaehle, S., Schürmann, G. J., Brovkin, V., Reick, C., and Schnur, R.: Separation of the Effects of Land and Climate Model Errors on Simulated Contemporary Land Carbon Cycle Trends in the MPI Earth System Model version 1, J. Climate, 28, 272–291, 2015.

Disney, M., Muller, J.-P., Kharbouche, S., **Kaminski**, **Thomas**., **Voßbeck**, **Michael**., Lewis, P., and Pinty, B.: A New Global fAPAR and LAI Dataset Derived from Optimal Albedo Estimates: Comparison with MODIS Products, Remote Sensing, 8, 275, doi:10.3390/rs8040275, http://www.mdpi.com/2072-4292/8/4/275, 2016.

European Commission, Joint Research Centre (JRC)/Netherlands Environmental Assessment Agency (PBL): Emission Database for Global Atmospheric Research (EDGAR), release version 4.0, http://edgar.jrc.ec.europa.eu,2009, 2009.

Farquhar, G., von Caemmerer, S., and Berry, J.: A biochemical model of photosynthetic CO2 assimilation in leaves of C3 species, Planta, 149, 78–90, doi:10.1007/BF00386231, 1980.

Forkel, M., Carvalhais, N., Schaphoff, S., v. Bloh, W., Migliavacca, M., Thurner, M., and Thonicke, K.: Identifying environmental controls on vegetation greenness phenology through model–data integration, Biogeosciences, 11, 7025–7050, doi:10.5194/bg-11-7025-2014, 2014.

Friedlingstein, P., Meinshausen, M., Arora, V. K., Jones, C. D., Anav, A., Liddicoat, S. K., and Knutti, R.: Uncertainties in CMIP5 Climate Projections due to Carbon Cycle Feedbacks, J. Climate, 27, 511–526, 2014.

Giering, R. and Kaminski, T.: Recipes for Adjoint Code Construction, ACM Trans. Math. Softw., 24, 437–474, doi:10.1145/293686.293695, 1998.

Giorgetta, M. A., Jungclaus, J., Reick, C. H., Legutke, S., Bader, J., Böttinger, M., Brovkin, V., Crueger, T., Esch, M., Fieg, K., Glushak, K., Gayler, V., Haak, H., Hollweg, H.-D., Ilyina, T., Kinne, S., Kornblueh, L., Matei, D., Mauritsen, T., Mikolajewicz, U., Mueller, W., Notz, D., Pithan, F., Raddatz, T., Rast, S., Redler, R., Roeckner, E., Schmidt, H., Schnur, R., Segschneider, J., Six, K. D., Stockhause, M., Timmreck, C., Wegner, J., Widmann, H., Wieners, K.-H., Claussen, M., Marotzke, J., and Stevens, B.: Climate and carbon cycle changes from 1850 to 2100 in MPI-ESM simulations for the Coupled Model Intercomparison Project phase 5, Journal of Advances in Modeling Earth Systems, 5, 572–597, doi:10.1002/jame.20038, 2013.

Gobron, N., Pinty, B., Melin, F., Taberner, M., Verstraete, M. M., Robustelli, M., and Widlowski, J.-L.: Evaluation of the MERIS/ENVISAT FAPAR product, Adv. Space Res., 39, 105–115, 2007.

Goll, D. S., Brovkin, V., Parida, B. R., Reick, C. H., Kattge, J., Reich, P. B., van Bodegom, P. M., and Niinemets, U.: Nutrient limitation reduces land carbon uptake in simulations with a model of combined carbon, nitrogen and phosphorus cycling, Biogeosciences, 9, 3547–3569, doi:10.5194/bg-9-3547-2012, 2012.

Griewank, A.: On Automatic Differentiation, in: Mathematical Programming: Recent Developments and Applications, edited by Iri, M. and Tanabe, K., pp. 83–108, Kluwer Academic Publishers, Dordrecht, 1989.

Gurney, K. R., Law, R. M., Denning, A. S., Rayner, P. J., Baker, D., Bousquet, P., Bruhwiler, L., Chen, Y.-H., Ciais, P., Fan, S., Fung, I. Y., Gloor, M., Heimann, M., Higuchi, K., John, J., Maki, T., Maksyutov, S., Masarie, K., Peylin, P., Prather, M., Pak, B. C., Randerson, J., Sarmiento, J., Taguchi, S., Takahashi, T., and Yuen, C.-W.: Towards robust regional estimates of CO2 sources and sinks using atmospheric transport models, Nature, 415, 626–630, 2002.

Hagemann, S. and Stacke, T.: Impact of the soil hydrology scheme on simulated soil moisture memory, Climate Dynamics, pp. 1–20, doi:10.1007/s00382-014-2221-6, 2014.

Heimann, M. and Körner, S.: The Global Atmospheric Tracer Model TM3, Tech. Rep. 5, Max-Planck-Institute for Biogeochemistry, 2003.

Houghton, R. A., House, J. I., Pongratz, J., van der Werf, G. R., DeFries, R. S., Hansen, M. C., Le Quéré, C., and Ramankutty, N.: Carbon emissions from land use and land-cover change, Biogeosciences, 9, 5125–5142, doi:10.5194/bg-9-5125-2012, 2012.

Jacobson, A. R., Mikaloff Fletcher, S. E., Gruber, N., Sarmiento, J. L., and Gloor, M.: A joint atmosphere-ocean inversion for surface fluxes of carbon dioxide: 1. Methods and global-scale fluxes, Global Biogeochemical Cycles, 21, n/a–n/a, doi:10.1029/2005GB002556, http://dx.doi.org/10.1029/2005GB002556, gB1019, 2007.

Jung, M., Vetter, M., Herold, M., Churkina, G., Reichstein, M., Zaehle, S., Ciais, P., Viovy, N., Bondeau, A., Chen, Y., Trusilova, K., Feser, F., and Heimann, M.: Uncertainties of modeling gross primary productivity over Europe: A systematic study on the effects of using different drivers and terrestrial biosphere models, Global Biogeochemical Cycles, 21, n/a–n/a, doi:10.1029/2006GB002915, gB4021, 2007.

Jung, M., Reichstein, M., Margolis, H. A., Cescatti, A., Richardson, A. D., Arain, M. A., Arneth, A., Bernhofer, C., Bonal, D., Chen, J., Gianelle, D., Gobron, N., Kiely, G., Kutsch, W., Lasslop, G., Law, B. E., Lindroth, A., Merbold, L., Montagnani, L., Moors, E. J., Papale, D., Sottocornola, M., Vaccari, F., and Williams, C.: Global patterns of land-atmosphere fluxes of carbon dioxide, latent heat, and sensible heat derived from eddy covariance, satellite, and meteorological observations, Journal of Geophysical Research: Biogeosciences, 116, n/a–n/a, doi:10.1029/2010JG001566, 2011.

Kalnay, E., Kanamitsu, M., Kistler, R., Collins, W., Deaven, D., Gandin, L., Iredell, M., Saha, S., White, G., Woollen, J., Zhu, Y., Leetmaa, A., Reynolds, R., Chelliah, M., Ebisuzaki, W., Higgins, W., Janowiak, J., Mo, K. C., Ropelewski, C., Wang, J., Jenne, R., and Joseph, D.: The NCEP/NCAR 40-Year Reanalysis Project, Bull. Amer. Meteor. Soc., 77, 437–471, 1996.

Kaminski, T. and Mathieu, P.-P.: Reviews and Syntheses: Flying the Satellite into Your Model, Biogeosciences Discussions, 2016, 1–25, doi:10.5194/bg-2016-237, http://www.biogeosciences-discuss.net/bg-2016-237/, 2016.

Kaminski, T., Heimann, M., and Giering, R.: A coarse grid three dimensional global inverse model of the atmospheric transport, 2, Inversion of the transport of CO_2 in the 1980s, J. Geophys. Res., 104, 18,555–18,581, 1999.

Kaminski, T., Giering, R., Scholze, M., Rayner, P., and Knorr, W.: A prototype of a data assimilation system based on automatic differentiation, Geophysical Research Abstracts, 5, 11 812, http://www.cosis.net/abstracts/EAE03/11812/EAE03-J-11812.pdf, 2003.

Kaminski, T., Knorr, W., Scholze, M., Gobron, N., Pinty, B., Giering, R., and Mathieu, P.-P.: Consistent assimilation of MERIS FAPAR and atmospheric CO_2 into a terrestrial vegetation model and interactive mission benefit analysis, Biogeosciences, 9, 3173–3184, doi:10.5194/bg-9-3173-2012, 2012.

Kaminski, T., Knorr, W., Schürmann, G., Scholze, M., Rayner, P. J., Zaehle, S., Blessing, S., Dorigo, W., Gayler, V., Giering, R., Gobron, N., Grant, J. P., Heimann, M., Hooker-Stroud, A., Houweling, S., Kato, T., Kattge, J., Kelley, D., Kemp, S., Koffi, E. N., Köstler, C., Mathieu, P.-P., Pinty, B., Reick, C. H., Rödenbeck, C., Schnur, R., Scipal, K., Sebald, C., Stacke, T., van Scheltinga, A. T., Vossbeck, M., Widmann, H., and Ziehn, T.: The BETHY/JSBACH Carbon Cycle Data Assimilation System: experiences and challenges, J. Geophys. Res. Biogeosci., 118, 1414–1426, 2013.

Kato, T., Knorr, W., Scholze, M., Veenendaal, E., Kaminski, T., Kattge, J., and Gobron, N.: Simultaneous assimilation of satellite and eddy covariance data for improving terrestrial water and carbon simulations at a semi-arid woodland site in Botswana, Biogeosciences, 10, 789–802, doi:10.5194/bg-10-789-2013, http://www.biogeosciences.net/10/789/2013/, 2013.

Kattge, J. and Knorr, W.: Temperature acclimation in a biochemical model of photosynthesis: a reanalysis of data from 36 species, Plant, Cell & Environment, 30, 1176–1190, doi:10.1111/j.1365-3040.2007.01690.x, 2007.

Kattge, J., Dí az, S., Lavorel, S., Prentice, I. C., Leadley, P., Bönisch, G., Garnier, E., Westoby, M., Reich, P. B., Wright, I. J., Cornelissen, J. H. C., Violle, C., Harrison, S. P., Van Bodegom, P. M., Reichstein, M., Enquist, B. J., Soudzilovskaia, N. A., Ackerly, D. D., Anand, M., Atkin, O., Bahn, M., Baker, T. R., Baldocchi, D., Bekker, R., Blanco, C. C., Blonder, B., Bond, W. J., Bradstock, R., Bunker, D. E., Casanoves, F., Cavender-Bares, J., Chambers, J. Q., Chapin III, F. S., Chave, J., Coomes,

D., Cornwell, W. K., Craine, J. M., Dobrin, B. H., Duarte, L., Durka, W., Elser, J., Esser, G., Estiarte, M., Fagan, W. F., Fang, J., Fernández-Méndez, F., Fidelis, A., Finegan, B., Flores, O., Ford, H., Frank, D., Freschet, G. T., Fyllas, N. M., Gallagher, R. V., Green, W. A., Gutierrez, A. G., Hickler, T., Higgins, S. I., Hodgson, J. G., Jalili, A., Jansen, S., Joly, C. A., Kerkhoff, A. J., Kirkup, D., Kitajima, K., Kleyer, M., Klotz, S., Knops, J. M. H., Kramer, K., Kühn, I., Kurokawa, H., Laughlin, D., Lee, T. D., Leishman, M., Lens, F., Lenz, T., Lewis, S. L., Lloyd, J., Llusià, J., Louault, F., MA, S., Mahecha, M. D., Manning, P., Massad, T., Medlyn, B. E., Messier, J., Moles, A. T., Müller, S. C., Nadrowski, K., Naeem, S., Niinemets, U., Nöllert, S., Nüske, A., Ogaya, R., Oleksyn, J., Onipchenko, V. G., Onoda, Y., Ordoñez, J., Overbeck, G., Ozinga, W. A., Patiño, S., Paula, S., Pausas, J. G., Peñuelas, J., Phillips, O. L., Pillar, V., Poorter, H., Poorter, L., Poschlod, P., Prinzing, A., Proulx, R., Rammig, A., Reinsch, S., Reu, B., Sack, L., Salgado-Negret, B., Sardans, J., Shiodera, S., Shipley, B., Siefert, A., Sosinski, E., Soussana, J.-F., Swaine, E., Swenson, N., Thompson, K., Thornton, P., Waldram, M., Weiher, E., White, M., White, S., Wright, S. J., Yguel, B., Zaehle, S., Zanne, A. E., and Wirth, C.: TRY – a global database of plant traits, Global Change Biology, 17, 2905–2935, doi:10.1111/j.1365-2486.2011.02451.x, http://dx.doi.org/10.1111/j.1365-2486.2011.02451.x, 2011.

Knauer, J., Werner, C., and Zaehle, S.: Evaluating stomatal models and their atmospheric drought response in a land surface scheme: A multi-biome analysis, Journal of Geophysical Research: Biogeosciences, pp. n/a–n/a, doi:10.1002/2015JG003114, 2015JG003114, 2015.

Knorr, W.: Satellite remote sensing and modelling of the global CO2 exchange of land vegetation: a synthesis study, Ph.D. thesis, Faculty of Earth Sciences of the University of Hamburg, 1997.

Knorr, W.: Annual and interannual CO2 exchanges of the terrestrial biosphere: process-based simulations and uncertainties, Global Ecology and Biogeography, 9, 225–252, 2000.

Knorr, W. and Heimann, M.: Uncertainties in global terrestrial biosphere modeling: 1. A comprehensive sensitivity analysis with a new photosynthesis and energy balance scheme, Global Biogeochemical Cycles, 15, 207–225, doi:10.1029/1998GB001059, 2001.

Knorr, W. and Kattge, J.: Inversion of terrestrial ecosystem model parameter values against eddy covariance measurements by Monte Carlo sampling, Global Change Biology, 11, 1333–1351, doi:10.1111/j.1365-2486.2005.00977.x, 2005.

Knorr, W., Kaminski, T., Scholze, M., Gobron, N., Pinty, B., Giering, R., and Mathieu, P.-P.: Carbon cycle data assimilation with a generic phenology model, J. Geophys. Res., 115, G04 017–, doi:10.1029/2009JG001119, 2010.

Knyazikhin, Y., Glassy, J., Privette, J. L., Tian, Y., Lotsch, A., Zhang, Y., Wang, Y., Morisette, J. T., Votava, P., Myneni, R., Nemani, R. R., and Running, S. W.: MODIS Leaf Area Index (LAI) and Fraction of Photosynthetically Active Radiation Absorbed by Vegetation (FPAR) Product (MOD15), Algorithm Theoretical Basis Document (ATBD), https://lpdaac.usgs.gov/products/modis_products_table/mcd15a2andhttp://modis.gsfc.nasa.gov/data/atbd/atbd_mod15.pdf, 1999.

Koffi, E. N., Rayner, P. J., Scholze, M., and Beer, C.: Atmospheric constraints on gross primary productivity and net ecosystem productivity: Results from a carbon-cycle data assimilation system, Global Biogeochemical Cycles, 26, n/a–n/a, doi:10.1029/2010GB003900, gB1024, 2012.

Kuppel, S., Peylin, P., Chevallier, F., Bacour, C., Maignan, F., and Richardson, A. D.: Constraining a global ecosystem model with multi-site eddy-covariance data, Biogeosciences, 9, 3757–3776, doi:10.5194/bg-9-3757-2012, 2012.

Kuppel, S., Chevallier, F., and Peylin, P.: Quantifying the model structural error in carbon cycle data assimilation systems, Geoscientific Model Development, 6, 45–55, doi:10.5194/gmd-6-45-2013, 2013.

Lasslop, G.: Model data fusion for terrestrial biosphere models with carbon and water cycle observations, Tech. Rep. 20, Max-Planck-Institut für Biogeochemie, P.O.Box 100164, 2011.

Lasslop, G., Thonicke, K., and Kloster, S.: SPITFIRE within the MPI Earth system model: Model development and evaluation, Journal of Advances in Modeling Earth Systems, 6, 740–755, doi:10.1002/2013MS000284, 2014.

Le Quéré, C., Moriarty, R., Andrew, R. M., Peters, G. P., Ciais, P., Friedlingstein, P., Jones, S. D., Sitch, S., Tans, P., Arneth, A., Boden, T. A., Bopp, L., Bozec, Y., Canadell, J. G., Chini, L. P., Chevallier, F., Cosca, C. E., Harris, I., Hoppema, M., Houghton, R. A., House, J. I., Jain, A. K., Johannessen, T., Kato, E., Keeling, R. F., Kitidis, V., Klein Goldewijk, K., Koven, C., Landa, C. S., Landschützer, P., Lenton, A., Lima, I. D., Marland, G., Mathis, J. T., Metzl, N., Nojiri, Y., Olsen, A., Ono, T., Peng, S., Peters, W., Pfeil, B., Poulter, B., Raupach, M. R., Regnier, P., Rödenbeck, C., Saito, S., Salisbury, J. E., Schuster, U., Schwinger, J., Séférian, R., Segschneider, J., Steinhoff, T., Stocker, B. D., Sutton, A. J., Takahashi, T., Tilbrook, B., van der Werf, G. R., Viovy, N., Wang, Y.-P., Wanninkhof, R., Wiltshire, A., and Zeng, N.: Global carbon budget 2014, Earth System Science Data, 7, 47–85, doi:10.5194/essd-7-47-2015, 2015.

Loew, A., van Bodegom, P. M., Widlowski, J.-L., Otto, J., Quaife, T., Pinty, B., and Raddatz, T.: Do we (need to) care about canopy radiation schemes in DGVMs? Caveats and potential impacts, Biogeosciences, 11, 1873–1897, doi:10.5194/bg-11-1873-2014, 2014.

Luke, C. M.: Modelling aspects of land-atmosphere interaction: Thermal instability in peatland soils and land parameter estimation through data assimilation, Ph.D. thesis, University of Exeter, U.K., 2011.

Luo, Y. Q., Randerson, J. T., Abramowitz, G., Bacour, C., Blyth, E., Carvalhais, N., Ciais, P., Dalmonech, D., Fisher, J. B., Fisher, R., Friedlingstein, P., Hibbard, K., Hoffman, F., Huntzinger, D., Jones, C. D., Koven, C., Lawrence, D., Li, D. J., Mahecha, M., Niu, S. L., Norby, R., Piao, S. L., Qi, X., Peylin, P., Prentice, I. C., Riley, W., Reichstein, M., Schwalm, C., Wang, Y. P., Xia, J. Y., Zaehle, S., and Zhou, X. H.: A framework for benchmarking land models, Biogeosciences, 9, 3857–3874, doi:10.5194/bg-9-3857-2012, 2012.

Mahecha, M. D., Reichstein, M., Carvalhais, N., Lasslop, G., Lange, H., Seneviratne, S. I., Vargas, R., Ammann, C., Arain, M. A., Cescatti, A., Janssens, I. A., Migliavacca, M., Montagnani, L., and Richardson, A. D.: Global Convergence in the Temperature Sensitivity of Respiration at Ecosystem Level, Science, 329, 838–840, doi:10.1126/science.1189587, http://science.sciencemag.org/content/329/5993/838, 2010.

Peylin, P., Law, R. M., Gurney, K. R., Chevallier, F., Jacobson, A. R., Maki, T., Niwa, Y., Patra, P. K., Peters, W., Rayner,

P. J., Rödenbeck, C., van der Laan-Luijkx, I. T., and Zhang, X.: Global atmospheric carbon budget: results from an ensemble of atmospheric CO_2 inversions, Biogeosciences, 10, 6699–6720, doi:10.5194/bg-10-6699-2013, 2013.

Piao, S., Sitch, S., Ciais, P., Friedlingstein, P., Peylin, P., Wang, X., Ahlström, A., Anav, A., Canadell, J. G., Cong, N., Huntingford, C., Jung, M., Levis, S., Levy, P. E., Li, J., Lin, X., Lomas, M. R., Lu, M., Luo, Y., Ma, Y., Myneni, R. B., Poulter, B., Sun, Z., Wang, T., Viovy, N., Zaehle, S., and Zeng, N.: Evaluation of terrestrial carbon cycle models for their response to climate variability and to CO2 trends, Global Change Biology, 19, 2117–2132, doi:10.1111/gcb.12187, 2013.

Pinty, B., Lavergne, T., Dickinson, R., Widlowski, J., Gobron, N., and Verstraete, M.: Simplifying the interaction of land surfaces with radiation for relating remote sensing products to climate models, J. Geophys. Res, 2006.

Pinty, B., Lavergne, T., Voßbeck, M., Kaminski, T., Aussedat, O., Giering, R., Gobron, N., Taberner, M., Verstraete, M. M., and Widlowski, J.-L.: Retrieving surface parameters for climate models from Moderate Resolution Imaging Spectroradiometer (MODIS)-Multiangle Imaging Spectroradiometer (MISR) albedo products, Journal of Geophysical Research: Atmospheres, 112, n/a–n/a, doi:10.1029/2006JD008105, http://dx.doi.org/10.1029/2006JD008105, d10116, 2007.

Pinty, B., Andredakis, I., Clerici, M., Kaminski, T., Taberner, M., Verstraete, M. M., Gobron, N., Plummer, S., and Widlowski, J.-L.: Exploiting the MODIS albedos with the Two-stream Inversion Package (JRC-TIP): 1. Effective leaf area index, vegetation, and soil properties, Journal of Geophysical Research: Atmospheres, 116, n/a–n/a, doi:10.1029/2010JD015372, 2011a.

Pinty, B., Clerici, M., Andredakis, I., Kaminski, T., Taberner, M., Verstraete, M. M., Gobron, N., Plummer, S., and Widlowski, J.-L.: Exploiting the MODIS albedos with the Two-stream Inversion Package (JRC-TIP): 2. Fractions of transmitted and absorbed fluxes in the vegetation and soil layers, Journal of Geophysical Research: Atmospheres, 116, n/a–n/a, doi:10.1029/2010JD015373, 2011b.

Pongratz, J., Reick, C., Raddatz, T., and Claussen, M.: A reconstruction of global agricultural areas and land cover for the last millennium, Global Biogeochemical Cycles, 22, n/a–n/a, doi:10.1029/2007GB003153, gB3018, 2008.

Press, W., Flannery, B., Teukolsky, S., and Vetterling, W.: Numerical Recipes in Fortran 77: The Art of Scientific Computing, Cambridge University Press, 1992.

Raddatz, T., Reick, C., Knorr, W., Kattge, J., Roeckner, E., Schnur, R., Schnitzler, K.-G., Wetzel, P., and Jungclaus, J.: Will the tropical land biosphere dominate the climate-carbon cycle feedback during the twenty-first century?, Climate Dynamics, 29, 565–574, doi:10.1007/s00382-007-0247-8, 2007.

Raupach, M. R., Rayner, P. J., Barrett, D. J., DeFries, R. S., Heimann, M., Ojima, D. S., Quegan, S., and Schmullius, C. C.: Model–data synthesis in terrestrial carbon observation: methods, data requirements and data uncertainty specifications, Global Change Biology, 11, 378–397, doi:10.1111/j.1365-2486.2005.00917.x, 2005.

Rayner, P. J., Enting, I. G., Francey, R. J., and Langenfelds, R. L.: Reconstructing the recent carbon cycle from atmospheric CO_2, $\delta^{13}C$ and O_2/N_2 observations, Tellus, 51B, 213–232, 1999.

Rayner, P. J., Scholze, M., Knorr, W., Kaminski, T., Giering, R., and Widmann, H.: Two decades of terrestrial carbon fluxes from a carbon cycle data assimilation system (CCDAS), Global Biogeochem. Cycles, 19, GB2026–, 2005.

Reick, C. H., Raddatz, T., Brovkin, V., and Gayler, V.: Representation of natural and anthropogenic land cover change in MPI-ESM, Journal of Advances in Modeling Earth Systems, 5, 459–482, doi:10.1002/jame.20022, 2013.

Rödenbeck, C., Houweling, S., Gloor, M., and Heimann, M.: CO_2 flux history 1982–2001 inferred from atmospheric data using a global inversion of atmospheric transport, Atmospheric Chemistry and Physics, 3, 1919–1964, doi:10.5194/acp-3-1919-2003, 2003.

Rödenbeck, C., Keeling, R. F., Bakker, D. C. E., Metzl, N., Olsen, A., Sabine, C., and Heimann, M.: Global surface-ocean p^{CO_2} and sea–air CO_2 flux variability from an observation-driven ocean mixed-layer scheme, Ocean Science, 9, 193–216, doi:10.5194/os-9-193-2013, 2013.

Roeckner, E., Bäuml, G., Bonaventura, L., Brokopf, R., Esch, M., Giorgetta, M., Hagemann, S., Kirchner, I., Kornblueh, L., Manzini, E., Rhodin, A., Schlese, U., Schulzweida, U., and Tompkins, A.: The atmospheric general circulation model ECHAM5 - Part 1: model description, Report 349, Max-Planck Institute for Meteorology, Hamburg, ISSN 0937 - 1060, 2003.

Saito, M., Ito, A., and Maksyutov, S.: Optimization of a prognostic biosphere model for terrestrial biomass and atmospheric CO_2 variability, Geoscientific Model Development, 7, 1829–1840, doi:10.5194/gmd-7-1829-2014, 2014.

Saugier, B. and Roy, J.: Estimations of Global Terrestrial Productivity: Converging Towards a Single Number?, in: Global Terrestrial Productivity: Past, Present and Future, edited by Mooney, H., Roy, J., and Saugier, B., Academic Press, San Diego, 2001.

Schneck, R., Reick, C. H., and Raddatz, T.: Land contribution to natural CO2 variability on time scales of centuries, Journal of Advances in Modeling Earth Systems, 5, 354–365, doi:10.1002/jame.20029, 2013.

Scholze, M., Kaminski, T., Rayner, P., Knorr, W., and Giering, R.: Propagating uncertainty through prognostic carbon cycle data assimilation system simulations, J. Geophys. Res., 112, D17 305–, 2007.

Sitch, S., Huntingford, C., Gedney, N., E., L. P., Lomas, M., Piao, S. L., Betts, R., Ciais, P., Cox, P., Friedlingstein, P., Jones, C. D., Prentice, I. C., and Woodward, F. I.: Evaluation of the terrestrial carbon cycle, future plant geography and climate-carbon cycle feedbacks using five Dynamic Global Vegetation Models (DGVMs), Global Change Biology, 14, 2015–2039, doi:10.1111/j.1365-2486.2008.01626.x, 2008.

Sitch, S., Friedlingstein, P., Gruber, N., Jones, S. D., Murray-Tortarolo, G., Ahlström, A., Doney, S. C., Graven, H., Heinze, C., Huntingford, C., Levis, S., Levy, P. E., Lomas, M., Poulter, B., Viovy, N., Zaehle, S., Zeng, N., Arneth, A., Bonan, G., Bopp, L., Canadell, J. G., Chevallier, F., Ciais, P., Ellis, R., Gloor, M., Peylin, P., Piao, S. L., Le Quéré, C., Smith, B., Zhu, Z., and Myneni, R.: Recent trends and drivers of regional sources and sinks of carbon dioxide, Biogeosciences, 12, 653–679, doi:10.5194/bg-12-653-2015, 2015.

Voßbeck, M., Clerici, M., Kaminski, T., Lavergne, T., Pinty, B., and Giering, R.: An inverse radiative transfer model of the vegetation

canopy based on automatic differentiation, Inverse Problems, 26, 095 003, 2010.

Weedon, G. P., Balsamo, G., Bellouin, N., Gomes, S., Best, M. J., and Viterbo, P.: The WFDEI meteorological forcing data set: WATCH Forcing Data methodology applied to ERA-Interim reanalysis data, Water Resources Research, 50, 7505–7514, doi:10.1002/2014WR015638, 2014.

Williams, M., Richardson, A. D., Reichstein, M., Stoy, P. C., Peylin, P., Verbeeck, H., Carvalhais, N., Jung, M., Hollinger, D. Y., Kattge, J., Leuning, R., Luo, Y., Tomelleri, E., Trudinger, C. M., and Wang, Y. P.: Improving land surface models with FLUXNET data, Biogeosciences, 6, 1341–1359, doi:10.5194/bg-6-1341-2009, 2009.

Zaehle, S., Sitch, S., Smith, B., and Hatterman, F.: Effects of parameter uncertainties on the modeling of terrestrial biosphere dynamics, Global Biogeochemical Cycles, 19, n/a–n/a, doi:10.1029/2004GB002395, gB3020, 2005.

Ziehn, T., Scholze, M., and Knorr, W.: On the capability of Monte Carlo and adjoint inversion techniques to derive posterior parameter uncertainties in terrestrial ecosystem models, Global Biogeochemical Cycles, 26, n/a–n/a, doi:10.1029/2011GB004185, http://dx.doi.org/10.1029/2011GB004185, gB3025, 2012.